HHS Public Access

Author manuscript

Cell Rep. Author manuscript; available in PMC 2024 September 30.

Published in final edited form as:

Cell Rep. 2024 July 23; 43(7): 114428. doi:10.1016/j.celrep.2024.114428.

The intracellular C-terminus confers compartment-specific targeting of voltage-gated calcium channels

Morven Chin[1], **Pascal S. Kaeser**[1,2,*]

[1]Department of Neurobiology, Harvard Medical School, Boston, MA 02115, USA

[2]Lead contact

SUMMARY

To achieve the functional polarization that underlies brain computation, neurons sort protein material into distinct compartments. Ion channel composition, for example, differs between axons and dendrites, but the molecular determinants for their polarized trafficking remain obscure. Here, we identify mechanisms that target voltage-gated Ca^{2+} channels (Ca_Vs) to distinct subcellular compartments. In hippocampal neurons, Ca_V2s trigger neurotransmitter release at the presynaptic active zone, and Ca_V1s localize somatoden-dritically. After knockout of all three Ca_V2s, expression of Ca_V2.1, but not Ca_V1.3, restores neurotransmitter release. We find that chimeric Ca_V1.3s with Ca_V2.1 intracellular C-termini localize to the active zone, mediate synaptic vesicle exocytosis, and render release sensitive to Ca_V1 blockers. This dominant targeting function of the Ca_V2.1 C-terminus requires the first EF hand in its proximal segment, and replacement of the Ca_V2.1 C-terminus with that of Ca_V1.3 abolishes Ca_V2.1 active zone localization and function. We conclude that Ca_V intracellular C-termini mediate compartment-specific targeting.

Graphical Abstract

*Correspondence: kaeser@hms.harvard.edu.

AUTHOR CONTRIBUTIONS

Conceptualization, M.C. and P.S.K.; methodology, M.C.; formal analysis, M.C. and P.S.K.; investigation, M.C.; resources, M.C.; writing – original draft, M.C. and P.S.K.; writing – review & editing, M.C. and P.S.K.; supervision, P.S.K.; funding acquisition, P.S.K.

SUPPLEMENTAL INFORMATION

Supplemental information can be found online at https://doi.org/10.1016/j.celrep.2024.114428.

DECLARATION OF INTERESTS

The authors declare no competing interests.

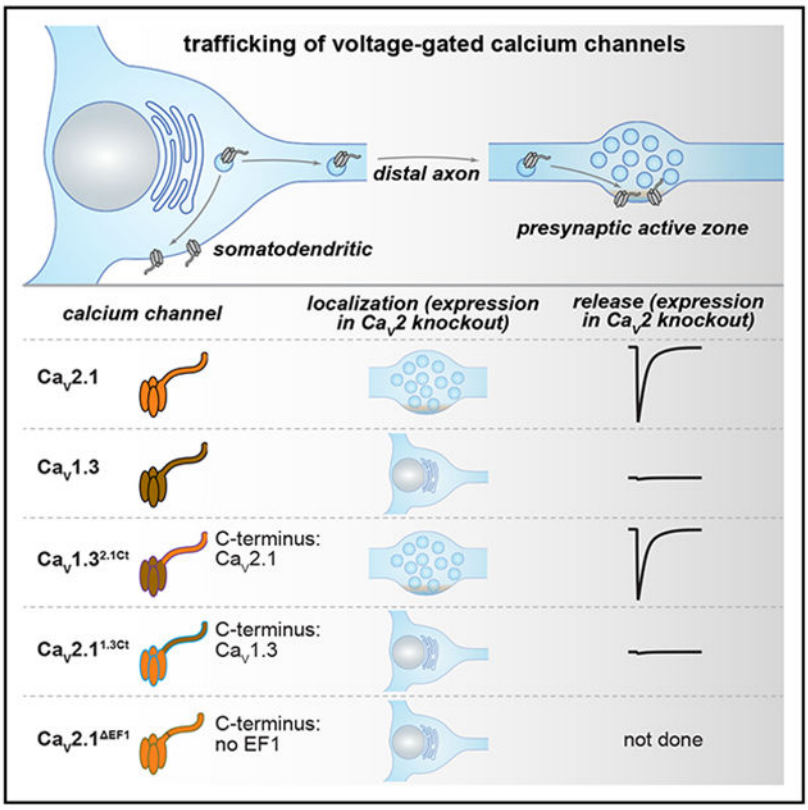

In brief

Voltage-gated Ca^{2+} channel subtypes are differentially sorted into the soma, dendrites, and axon of a neuron. Chin et al. find that the intracellular C-termini of Ca_V1 and Ca_V2 channels are key determinants for compartment targeting and report an essential trafficking role for the first EF hand of $Ca_V2.1$.

INTRODUCTION

Neurons are polarized cells with a defined signaling directionality from dendrites to soma to axon.[1] To achieve this morphological and functional polarization, neurons sort protein material into specific subcellular compartments.[2,3] Voltage-gated Ca^{2+} channels (Ca_Vs), which couple electrical activity to intracellular Ca^{2+} signaling, are a prototypical example of sorting specificity. They are a large protein family, and individual members localize to distinct subcellular domains in the dendrites, soma, and axon.[4,5] However, Ca_V subtypes exhibit limited sequence differences, and the molecular determinants that target Ca_Vs to specific compartments remain elusive.

Ca_Vs are defined by their pore-forming $Ca_V\alpha1$ subunit, and their expression, trafficking, and function are modulated by $Ca_V\beta$ subunits and $Ca_V\alpha2\delta$ proteins.[4-7] Vertebrate $Ca_V\alpha1$ subunits are encoded by ten genes classified into Ca_V1 ($Ca_V1.1$–1.4, L-type), Ca_V2 ($Ca_V2.1$–2.3, P/Q-, N-, and R-type), and Ca_V3 ($Ca_V3.1$–3.3, T-type) channels. Most Ca_Vs are co-expressed in central neurons. $Ca_V1.2$ and $Ca_V1.3$ have important roles in

the somatodendritic compartment, and their activity there regulates gene transcription[8-11] and modulates neuronal firing directly and through Ca^{2+}-activated K^+ channels.[12-16] In presynaptic nerve terminals, $Ca_V2.1$ (P/Q-type) and $Ca_V2.2$ (N-type) channels are the primary Ca^{2+} sources for synaptic vesicle release.[17-20] They are recruited to a specialized release apparatus, the active zone, where they are tethered near fusion-competent vesicles.[21-25] This organization couples action potential-induced Ca^{2+} entry to vesicular release sites for triggering of neurotransmitter exocytosis. Overall, Ca_Vs contribute to diverse cellular processes, and their functions are directly tied to their subcellular localization.

The mechanisms that distinguish Ca_V1s from Ca_V2s and sort them into the somatodendritic and axonal compartments, respectively, remain unclear. Starting from their primary site of synthesis in the soma, Ca_Vs likely undergo a series of interactions that target each subtype to its respective subcellular domain.[2,26] However, Ca_Vs are highly similar in structure,[5,27,28] and notable overlap exists within the Ca_V1 and Ca_V2 interactome. For example, interactions with $Ca_V\beta$, $Ca_V\alpha2\delta$, and calmodulin have been implicated in Ca_V trafficking,[29-36] but these proteins interact indiscriminately with Ca_V1s and Ca_V2s and are thus unlikely to encode specific sorting information.

The intracellular Ca_V C-termini might mediate targeting specificity. Ca_V C-termini include a proximal segment with two EF hands and an IQ motif, and a distal segment containing binding sites for scaffolding proteins (Figures S1A and S1B). The Ca_V2 C-terminus binds to the PDZ domain of the active zone protein RIM, and it contains a proline-rich sequence (which is also present in Ca_V1s) that binds to RIM-binding protein (RIM-BP).[24,37,38] These distal C-terminal sequences help tether Ca_V2s to the presynaptic active zone.[20,24,39-44] Analogous sequences in $Ca_V1.3$ bind to the postsynaptic scaffold Shank, and overall, Ca_V1 C-termini support cell surface expression and the assembly of dendritic Ca_V1 clusters.[45,46] A $Ca_V2.1$-specific sequence stretch between the proximal C-terminus and the RIM-BP binding site contributes redundantly to $Ca_V2.1$ localization alongside the C-terminal interactions with RIM and RIM-BP.[20,47] Important roles for Ca_V2 C-termini in channel trafficking are further supported by the finding that $Ca_V2.1$ is absent from nerve terminals when its C-terminus is fully removed[20] and by a recent report that $Ca_V2.1$ channels with the C-terminus of $Ca_V2.3$ exhibit impaired presynaptic abundance.[48]

Sequences outside the Ca_V C-terminus could also be involved. For example, binding of the synprint motif in the Ca_V2 cytoplasmic II-III loop to SNARE proteins may contribute to release site recruitment.[49-51] However, channels lacking this sequence retain presynaptic targeting, and synprint inhibitory peptides can act independently of the synprint motif.[52,53] Interactions with material in the synaptic cleft may also mediate active zone anchoring.[54,55] Taken together, multiple interactions have been implicated in Ca_V trafficking and targeting, but how these interactions direct Ca_V1s and Ca_V2s to opposing compartments has remained unclear.

Here, we found that the Ca_V C-termini are the primary determinants of compartment targeting in hippocampal neurons. Swapping the $Ca_V2.1$ C-terminus onto $Ca_V1.3$ targets the channel to the presynaptic active zone in Ca_V2 knockout neurons. This chimeric $Ca_V1.3$

channel mediates Ca^{2+} entry for neurotransmitter release and renders synaptic vesicle exocytosis sensitive to L-type Ca_V blockers. In contrast, the reverse swap prevents active zone localization and function of $Ca_V2.1$. Within the $Ca_V2.1$ proximal C-terminus, the first EF hand is required for presynaptic targeting, and its removal leads to loss of $Ca_V2.1$ from the active zone. We conclude that the C-terminus specifies Ca_V localization, and we identify the first EF hand as an essential trafficking motif.

RESULTS

Exogenous $Ca_V2.1$, but not $Ca_V1.3$, localizes to active zones and mediates neurotransmitter release after Ca_V2 ablation

To determine the Ca_V sequences important for active zone localization, we expressed various Ca_Vs using lentiviruses in cultured hippocampal neurons that lack $Ca_V2.1$, $Ca_V2.2$, and $Ca_V2.3$. Specifically, we transduced neurons that contain “floxed” conditional knockout alleles for these three channels (Figure 1A) with lentiviruses that express cre recombinase under a synapsin promoter to generate Ca_V2 cTKO neurons.[20] Control neurons (Ca_V2 control) were identical except for transduction by a lentivirus expressing a truncated, recombination-deficient version of cre. In addition, we transduced Ca_V2 cTKO neurons with a lentivirus expressing either hemagglutinin (HA)-tagged $Ca_V2.1$ or HA-tagged $Ca_V1.3$. The HA tag was inserted near the Ca_V N-terminus in a position shown previously to not interfere with the expression (Figures 1B and S1A-1E), targeting, and function of $Ca_V2.1$.[20,56] We then used stimulated emission depletion (STED) microscopy (Figures 1C-1H), confocal microscopy (Figures S1F-S1I), and electrophysiology (Figures 1I-1L) to assess Ca_V localization and synaptic transmission.

For morphological analyses, neurons were stained with antibodies against $Ca_V2.1$ or HA to detect Ca_Vs, PSD-95 to mark postsynaptic densities, and synapsin to label synaptic vesicle clusters. For STED analyses (Figures 1C-1H), we selected synapses in side view through the presence of a vesicle cloud (imaged with confocal microscopy) and an elongated PSD-95 structure (imaged with STED microscopy) at one edge of the vesicle cloud, as established previously.[20,25,40,41,57] We assessed Ca_V distribution and levels in STED images of these side-view synapses using line profiles perpendicular to PSD-95, and we plotted the average profiles (Figures 1D and 1G) and peak intensities (Figures 1E and 1H).

Endogenous and re-expressed $Ca_V2.1$ formed elongated structures apposed to PSD-95 with a maximal intensity within tens of nanometers of the PSD-95 peak (Figures 1C-1H). We have established before that this distribution is characteristic of active zone localization.[20,25,41,58] Furthermore, a strong PSD-95 peak was present in all conditions, matching our previous work that did not find morphological defects following Ca_V2 triple knockout.[20] Exogenously expressed $Ca_V1.3$, monitored via the HA tag, was not detected at the active zone (Figures 1F-1H). Consistent with the STED analyses, confocal microscopy revealed robust levels of $Ca_V2.1$, but not $Ca_V1.3$, in synaptic regions of interest (ROIs) defined by synapsin (Figures S1F-S1I). Independent of their synaptic targeting, both $Ca_V2.1$ and $Ca_V1.3$ were effectively expressed in the somata of transduced Ca_V2 cTKO neurons and in transfected HEK293T cells (Figures S1C-S1E).

These morphological experiments were complemented with analyses of synaptic transmission (Figures 1I-1L). A focal stimulation electrode was used to evoke action potentials, and inhibitory or excitatory postsynaptic currents (IPSCs or EPSCs, respectively) were isolated pharmacologically. EPSCs were monitored via NMDA receptors because network excitation confounds the interpretation of EPSC amplitudes when AMPA receptors are not blocked. Ca_V2 cTKO nearly abolished evoked synaptic transmission, as characterized in detail before.[20] Re-expression of $Ca_V2.1$ restored EPSCs and IPSCs effectively, but exogenous expression of $Ca_V1.3$ failed to produce any recovery (Figures 1I-1L), in agreement with the absence of $Ca_V1.3$ from presynaptic sites (Figures 1F-1H, S1H, and S1I). Taken together, these results establish that exogenously expressed $Ca_V2.1$, but not $Ca_V1.3$, localizes to the active zone and gates neurotransmitter release in Ca_V2 cTKO neurons.

$Ca_V1.3$ chimeras that contain the $Ca_V2.1$ C-terminus localize to the active zone

Given the diverse interactions that converge within the Ca_V C-termini (Figures S1A and S1B),[20,44,45] we hypothesized that the C-terminal sequences contain sufficient information to instruct Ca_V compartment specificity. To test this hypothesis, we generated two chimeric Ca_Vs. In $Ca_V1.3$, we replaced the intracellular C-terminus immediately after the last transmembrane segment with that of $Ca_V2.1$, generating a channel we named $Ca_V1.3^{2.1Ct}$. We also produced the inverse construct by replacing the $Ca_V2.1$ C-terminus with that of $Ca_V1.3$, generating $Ca_V2.1^{1.3Ct}$ (Figures 2A and S1A). Both chimeric channels were efficiently expressed in transfected HEK293T cells and robustly detected in neuronal somata following lentiviral transduction of Ca_V2 cTKO neurons (Figure S2).

We then assessed the localization of these chimeric channels in the experimental setup described above and compared them side by side with $Ca_V2.1$ and $Ca_V1.3$. Strikingly, translocating the $Ca_V2.1$ C-terminus onto $Ca_V1.3$ efficiently targeted the resulting chimeric $Ca_V1.3^{2.1Ct}$ channel to the active zone in Ca_V2 cTKO neurons, as assessed with STED microscopy (Figures 2B-2D). The distribution profile of $Ca_V1.3^{2.1Ct}$ and its abundance at the active zone recapitulated those of re-expressed $Ca_V2.1$ (Figures 2B-2D). In contrast, the inverse swap abolished active zone localization of $Ca_V2.1^{1.3Ct}$ (Figures 2B-2D) despite effective somatic expression (Figures S2B and S2C). Confocal microscopic analyses of Ca_V levels in synaptic ROIs corroborated these findings by revealing robust synaptic localization of $Ca_V1.3^{2.1Ct}$ but not $Ca_V2.1^{1.3Ct}$ (Figures 2E and 2F).

These results establish that $Ca_V1.3$ is targeted to the presynaptic active zone when its C-terminus is replaced with that of $Ca_V2.1$. Conversely, $Ca_V2.1$ loses its active zone localization following the reverse swap. We conclude that the Ca_V C-termini contain sufficient information to define Ca_V compartment specificity, and these and previous data lead to two predictions. First, because removing known scaffolding motifs in the distal C-terminus only partially impaired active zone localization,[20,47] there must be essential targeting motifs in the Ca_V C-terminus that have not yet been identified. Second, if the chimeric $Ca_V1.3^{2.1Ct}$ channel is appropriately coupled to primed vesicles within the active zone, then $Ca_V1.3^{2.1Ct}$ expression should restore synaptic transmission in Ca_V2 cTKO

neurons and render neurotransmitter release sensitive to L-type channel blockade. We next tested both predictions.

The first EF hand in the proximal C-terminus is necessary for Ca_V2 active zone targeting

Removal of the known active zone scaffolding motifs in the $Ca_V2.1$ C-terminus produced a partial defect in $Ca_V2.1$ active zone targeting, but truncation of the entire C-terminus fully abolished active zone localization.[20] To define C-terminal sequences that contain unidentified targeting motifs, we segregated the $Ca_V2.1$ C-terminus into a distal segment containing the active zone scaffolding motifs and a complementary proximal segment (Figures S1A and S1B). We generated two additional $Ca_V1.3$ chimeras (Figure 3A) by translocating either only the $Ca_V2.1$ proximal ($Ca_V1.3^{2.1ProxCt}$) or distal ($Ca_V1.3^{2.1DistCt}$) C-terminus onto $Ca_V1.3$. $Ca_V1.3^{2.1ProxCt}$ and $Ca_V1.3^{2.1DistCt}$ were expressed efficiently in HEK293T cells after transfection and in neuronal somata after lentiviral transduction (Figures S3A-S3C). With STED microscopy, we detected $Ca_V1.3^{2.1ProxCt}$ at the active zone (Figures 3B-3D) of Ca_V2 cTKO neurons. Active zone levels of $Ca_V1.3^{2.1ProxCt}$ were reduced compared to $Ca_V1.3^{2.1Ct}$ levels and resembled those of a mutant $Ca_V2.1$ that lacks the active zone scaffolding motifs in the distal C-terminus.[20] Hence, active zone targeting of chimeric $Ca_V1.3$s operates in part through these distal sequences. Accordingly, $Ca_V1.3^{2.1DistCt}$ exhibited strong active zone localization in Ca_V2 cTKO neurons and was indistinguishable from $Ca_V1.3^{2.1Ct}$ (Figures 3B-3D). Confocal analyses of protein levels in synaptic ROIs matched these findings (Figures S3D and S3E).

$Ca_V1.3^{2.1ProxCt}$ demonstrates that translocation of the $Ca_V2.1$ proximal C-terminus onto $Ca_V1.3$ suffices to mediate some active zone localization (Figures 3B-3D) and indicates that the proximal C-terminal sequences are important for presynaptic trafficking. Ca_V proximal C-termini (Figures S1A and S1B) contain two EF hands.[28,59] The first EF hand has been implicated in calmodulin-dependent modulation of Ca_V function,[60-62] though no evidence to date establishes a role in Ca_V trafficking. We tested whether the first EF hand mediates active zone targeting by deleting it from $Ca_V2.1$ ($Ca_V2.1^{\Delta EF1}$; Figure 3E). $Ca_V2.1^{\Delta EF1}$ was readily expressed in transfected HEK293T cells and detected in somata of lentivirally transduced neurons (Figures S3F-S3H). However, deleting this EF hand abolished $Ca_V2.1$ active zone localization in STED microscopy (Figures 3F-3H) and rendered $Ca_V2.1^{\Delta EF1}$ undetectable at synapses in confocal microscopy (Figures S3I and S3J).

In summary, the $Ca_V2.1$ distal C-terminus needs to be paired with proximal C-terminal elements to effectively localize Ca_Vs to the active zone. Our data establish that the first EF hand is required for active zone targeting of $Ca_V2.1$.

$Ca_V1.3^{2.1Ct}$ supports neurotransmitter release and confers L-type blocker sensitivity after Ca_V2 ablation

Having demonstrated that translocation of the $Ca_V2.1$ C-terminus directs $Ca_V1.3$ to the active zone, we asked whether $Ca_V1.3^{2.1Ct}$ provides Ca^{2+} for triggering synaptic vesicle exocytosis (Figure 4A). We first evaluated $Ca_V1.3^{2.1Ct}$ by characterizing its activity in transfected HEK293T cells. $Ca_V1.3^{2.1Ct}$ conducted robust inward currents, and $Ca_V1.3^{2.1Ct}$ and $Ca_V1.3$ exhibited similar voltage dependency (Figures S4A-S4C). When expressed

in Ca_V2 cTKO neurons, $Ca_V1.3^{2.1Ct}$ restored evoked EPSCs (Figures 4B and 4C) and IPSCs (Figures 4D and 4E) as well as decreases in miniature EPSC (mEPSC) and mIPSC frequencies,[20] as did $Ca_V2.1$ (Figures S4D-S4G). These data establish that $Ca_V1.3^{2.1Ct}$ is coupled to the presynaptic release machinery to gate neurotransmitter release. In contrast, and consistent with the loss of active zone targeting in neurons (Figures 2B-2D) and the inability to mediate inward currents in HEK293T cells (Figures S4A-S4C), $Ca_V2.1^{1.3Ct}$ failed to restore evoked synaptic transmission (Figures 4B-4E).

It is possible that $Ca_V1.3^{2.1Ct}$ presynaptic targeting and function result from the removal of a dendritic targeting sequence rather than the addition of an axonal targeting motif. To address this possibility, we generated a $Ca_V1.3$ lacking the entire C-terminus ($Ca_V1.3^{\Delta Ct}$). $Ca_V1.3^{\Delta Ct}$ was effectively expressed (Figures S5A-S5D) but not targeted to synapses (Figures S5E and S5F) or active zones (Figures S5G-S5I). Furthermore, $Ca_V1.3^{\Delta Ct}$ did not mediate neurotransmitter release (Figures S5J-S5M). We conclude that active zone targeting of $Ca_V1.3^{2.1Ct}$ arises from an instructive role of the $Ca_V2.1$ C-terminus.

At central synapses, neurotransmitter release is insensitive to L-type Ca_V blockade (Figures S4H-S4J).[17] Given that we replaced presynaptic Ca_V2s with the L-type-like $Ca_V1.3^{2.1Ct}$, we tested whether we also altered the pharmacological sensitivity of synaptic transmission. We performed serial Ca_V blockade (Figure 4F) through sequential application of ω-agatoxin IVA (ω-agatoxin, to block $Ca_V2.1$) and isradipine (to block Ca_V1s). In Ca_V2 control neurons, ω-agatoxin reduced IPSCs by half (Figures 4G-4I), consistent with the reliance of these synapses on both $Ca_V2.1$ and $Ca_V2.2$.[20,24,63] Isradipine had no effect in Ca_V2 control neurons (Figures S4H-S4J). Naturally, ω-agatoxin fully inhibited synaptic transmission in Ca_V2 cTKO neurons rescued with $Ca_V2.1$. However, for Ca_V2 cTKO neurons that expressed $Ca_V1.3^{2.1Ct}$, synaptic transmission was resistant to ω-agatoxin and instead wholly sensitive to isradipine (Figures 4G-4I). Hence, $Ca_V1.3^{2.1Ct}$ functionally incorporates into release machinery in Ca_V2 cTKO neurons and renders neurotransmission fully dependent on L-type Ca_V activity.

DISCUSSION

Distinct Ca_Vs are sorted effectively to somatodendritic and axonal compartments. Here, we establish that the Ca_V C-termini contain necessary and sufficient information for compartment sorting. Within the C-terminus of $Ca_V2.1$, the first EF hand is essential for presynaptic targeting, and it operates in concert with distal scaffolding motifs. Together, the $Ca_V2.1$ C-terminal sequences are sufficient to re-direct somatodendritic Ca_V1 channels to the active zone of axonal nerve terminals. Conversely, the $Ca_V1.3$ C-terminal sequences disrupt $Ca_V2.1$ active zone localization and its function. Our work establishes mechanisms for compartment-specific targeting of a protein family central to the polarized organization of neurons.

Forward trafficking of Ca_Vs

Multiple cargo selectivity filters within the endoplasmic reticulum, Golgi apparatus, axon initial segment, and presynaptic boutons together permit the targeting of a limited subset of proteins to the active zone while deflecting other cargo.[64,65] Sequence motifs within these

proteins may dictate compartment sorting at two major checkpoints: (1) they may mediate protein recruitment into cargo vesicles directed to the axon, and (2) they may stabilize proteins at the active zone following their delivery.[2,66] Our work establishes that the $Ca_V2.1$ C-terminus encodes necessary and sufficient information to navigate these check-points and implies a cooperative relationship between the proximal and distal elements. The $Ca_V2.1$ distal C-terminus efficiently localizes chimeric $Ca_V1.3$s to the active zone, indicating that the distal sequences permit both Ca_V sorting into presynaptic cargo and Ca_V tethering at the active zone, so long as the first EF hand is present. The distal motifs that bind to active zone proteins likely fulfill these roles, as disrupting their interactions with RIM and RIM-BP leads to targeting defects,[20,24,38,39,41,47] similar to those exhibited by chimeric $Ca_V1.3$s with the $Ca_V2.1$ proximal C-terminus and the $Ca_V1.3$ distal C-terminus (Figure 3).

Both $Ca_V1.3^{2.1Ct}$ and $Ca_V1.3^{2.1DistCt}$ are efficiently targeted to the active zone, which establishes that the $Ca_V1.3$ and $Ca_V2.1$ proximal C-termini contain information for Ca_V active zone delivery when paired with the $Ca_V2.1$ distal scaffolding motifs. This is in line with the high homology of the EF hands and IQ motif across Ca_V proximal C-termini and the presence of these sequences in other voltage-gated channels.[28,67] The proximal C-terminus might provide multiple instructive signals. For example, the first EF hand binds AP-1, and the IQ motif binds calmodulin, and these interactions could serve as trafficking control checkpoints.[33,34,68,69] Proximal C-terminal sequences are also involved in Ca^{2+}-dependent signaling,[60-62] but any contributions to trafficking are likely independent of these functions as perturbations of Ca^{2+} influx and neuronal firing do not disrupt presynaptic Ca_V abundance.[20] Unknown interactions of the proximal C-terminus may be involved in targeting as well. Altogether, we posit that the first EF hand is necessary for the incorporation of Ca_Vs into axon-bound cargo, but it likely has no role afterward in stabilizing Ca_Vs within the active zone.

C-terminal sequences for regulating Ca_V abundance at the active zone

Ca_V2 active zone targeting may be regulated by the availability of channel slots, which may impose an upper limit on presynaptic Ca_V abundance and may prefer specific Ca_V subtypes.[70,71] We found that $Ca_V2.1$ and $Ca_V1.3^{2.1Ct}$ restored active zone Ca_V abundance and neurotransmitter release with similar efficacy when expressed in Ca_V2 cTKO neurons. Importantly, synaptic transmission in these neurons and in Ca_V2 control neurons was comparable (Figures 2, 4, and S4). Hence, Ca_Vs with the $Ca_V2.1$ C-terminus effectively occupy available Ca_V slots in terminals without endogenous Ca_V2s. In contrast, recent work revealed that swapping the $Ca_V2.3$ C-terminus onto $Ca_V2.1$ decreased channel abundance at the calyx of Held,[48] suggesting that the $Ca_V2.3$ C-terminus does not efficiently target channels to the same slots. Overall, the $Ca_V2.1$ C-terminus mediates efficient slot occupancy, and Ca_V2 C-termini may also define slot preference.

Ca_V2 alternative splicing may confer further diversity. Ca_V2 C-termini contain multiple splice sites that may regulate channel trafficking.[72,73] For example, alternative splicing can remove the distal scaffolding motifs necessary for efficient active zone tethering.[20,72] In $Ca_V2.2$s, splicing within the first EF hand can disrupt an AP-1 binding site, possibly

impeding forward trafficking.[68] In summary, Ca_Vs undergo extensive alternative splicing, but how splicing modulates Ca_V localization and function remains unclear.

Limitations of the study

Because we characterized $Ca_V2.1$, $Ca_V1.3$, and their derivative chimeric channels in Ca_V2 cTKO neurons, we did not assess the relative contributions of endogenous $Ca_V2.1$, $Ca_V2.2$, and $Ca_V2.3$ to evoked and spontaneous neurotransmitter release or the possibility of subtype-preferring slots.[17-20,70,71,74-79] Ca_V2 channels can exhibit some somatodendritic activity and localization.[80-83] The underlying targeting mechanisms are unknown, and it remains uncertain whether this localization arises from active somatodendritic retention. Further, we utilize virally expressed Ca_V cDNAs for rescue, which prevents alternative splicing that may further modulate channel abundance, localization, and function.[61,68,72,73,84] Finally, the cultured neurons were mixed from neonatal mice of both sexes and cannot be used to assess sex-specific phenotypes.

Nevertheless, our work provides mechanistic insight into the polarized trafficking of protein material in neurons and raises multiple questions. First, some synapses depend on only a single Ca_V2 subtype, while others use multiple Ca_V2s, and some synapses experience developmental switches in Ca_V2 usage.[85,86] Whether there are specific trafficking mechanisms or whether these properties are determined wholly by switches in gene expression remains to be determined. Second, the proximal sequences we identified as important for targeting are also present in other ion channels that undergo polarized trafficking, for example in Na^+ channels.[28,67] It is possible that the mechanisms we describe for Ca_Vs are employed by other channels, and Ca_Vs represent an ideal framework to further define mechanisms that sort proteins into specific neuronal compartments.

STAR★METHODS

RESOURCE AVAILABILITY

Lead contact—Further information and requests for resources and reagents should be directed to and will be fulfilled by the lead contact, Pascal S. Kaeser (kaeser@hms.harvard.edu).

Materials availability—Plasmids generated for this study will be shared upon request. Mouse lines and previously generated plasmids will be shared upon request within the limits of the respective material transfer agreements.

Data and code availability

- Data reported in this paper will be shared by the lead contact upon request. A table with numerical data has been deposited at Zenodo and is available at https://doi.org/10.5281/zenodo.11583935.
- This paper does not report original code.
- Any additional information required to reanalyze the data reported in this paper is available from the lead contact upon request.

EXPERIMENTAL MODEL AND SUBJECT DETAILS

Mice—Ca_V2 conditional triple homozygote floxed mice were described before[20] and they contain homozygote floxed alleles for $Ca_V2.1$ (*Cacna1a*,[87]), $Ca_V2.2$ (*Cacna1b*,[20]), and $Ca_V2.3$ (*Cacna1e*,[88]). Adult mice were either separated by sex, or housed as breeding pairs, and they were under a 12 h light-dark cycle with free access to food and water in a room set to 22°C (range 20°C–24°C) and 50% humidity (range 35–70%). Mice were genotyped either in the lab following established protocols[20] or by Transnetyx. For *Cacna1a*, the following oligonucleotide primer pair was used for in-lab genotyping: forward, ACCTACAGTCTGCCAGGAG; reverse, TGAAGCCCAGACATCCTTGG (expected band sizes, wild type: 393 bp, floxed: 543 bp); for *Cacna1b*: forward, TGGTTGG TGTCCTGTTCTCC; reverse, TAAGGAGCAGGGAATCCTGG (expected band sizes, wild type: 219bp, floxed: 359 bp); for *Cacna1c*: forward, GACAAGACCCCAATGTCTCG; reverse, TCCATGTTCCTTCTCACTCC (expected band sizes, wild type: 295 bp, floxed: 334 bp). Animal experiments were performed according to approved protocols at Harvard University.

Primary neuronal cultures—Primary mouse hippocampal cultures were generated from newborn mice as established before.[20,40,41] Hippocampi were dissected out from newborn mice within 24 h after birth. Cells were dissociated and plated onto Matrigel-treated glass coverslips in plating medium composed of Minimum Essential Medium (MEM) with 0.5% glucose, 0.02% NaHCO3, 0.1 mg/mL transferrin, 10% Fetal Select bovine serum (Atlas Biologicals FS-0500-AD), 2 mM L-glutamine, and 25 μg/mL insulin. Cells from mice of both sexes were mixed. Cultures were maintained in a 37°C-tissue culture incubator, and after ~24 h the plating medium was exchanged with growth medium composed of MEM with 0.5% glucose, 0.02% NaHCO3, 0.1 mg/mL transferrin, 5% Fetal Select bovine serum (Atlas Biologicals FS-0500-AD), 2% B-27 supplement (Thermo Fisher 17504044), and 0.5 mM L-glutamine. On day *in vitro* (DIV) 1 to 2, depending on growth, 50% or 75% of the medium was exchanged with growth medium supplemented with 4 μM Cytosine β-D-arabinofurano-side (AraC). Experiments and analyses were performed at DIV15 to 19.

Cell lines—HEK293T cells, an immortalized cell line of female origin, were cultured as established before.[20,40,41] They were purchased from ATCC (CRL-3216, RRID: CVCL_0063), expanded, and stored in liquid nitrogen until use. After thawing, the cells were grown in Dulbecco's Modified Eagle Medium with 10% fetal bovine serum (Atlas Biologicals F-0500-D) and 1% penicillin-streptomycin. HEK293T cells were passaged every 1 to 3 d at a ratio of 1:3 to 1:10. HEK293T cell batches were typically replaced after 20 passages by thawing a fresh vial from the expanded stock.

METHOD DETAILS

Lentiviruses—Lentiviruses used to transduce primary hippocampal neurons were produced in HEK293T cells. HEK293T cells were transfected with the Ca^{2+} phosphate method with REV (p023), RRE (p024) and VSVG (p025), as well as a lentiviral plasmid encoding the protein of interest. For Ca_V proteins of interest, these were plasmids p789, p947, p1077, p1078, p1079, p1080, p1083, and p1084. To produce lentiviruses expressing EGFP-tagged Cre recombinase (to generate Ca_V2 cTKO neurons), pFSW EGFP-Cre (p009)

was used. For lentiviruses expressing a truncated, enzymatically inactive EGFP-tagged Cre (to generate Ca_V2 control neurons), pFSW EGFP-ΔCre (p010) was used. Plasmids were transfected at a 1:1:1:1 molar ratio and with a total amount of 6.7 μg DNA. Approximately 24 h after transfection, the medium was switched to neuronal growth medium (described above), and the HEK293T cell supernatant was harvested 24–36 h later by centrifugation at 700 x g. For expression of EGFP-Cre and EGFP-ΔCre, neurons were transduced by adding HEK293T cell supernatant at DIV5. For expression of Ca_Vs, neurons were transduced at DIV1. Ca_V2 control neurons were additionally transduced with a virus made using a pFSW plasmid (p008) lacking a cDNA in the multiple cloning site in place of an expression virus. Neuronal protein expression from these lentiviruses was driven by the human synapsin I promoter.[40,89]

Ca_V expression constructs—For experiments in neurons, lentiviral backbones containing the human synapsin I promoter were used (pFSW HA-$Ca_V2.1$, p789; pFSW HA-$Ca_V2.1^{\Delta EF1}$, p947; pFSW HA-$Ca_V1.3$, p1077; pFSW HA-$Ca_V1.3^{2.1Ct}$, p1078; pFSW HA-$Ca_V2.1^{1.3Ct}$, p1079; pFSW HA-$Ca_V1.3^{\Delta Ct}$, p1080; pFSW HA-$Ca_V1.3^{2.1ProxCt}$, p1083; pFSW HA-$Ca_V1.3^{2.1DistCt}$, p1084). For experiments in HEK293T cells, expression vectors with a CMV promoter were used (pCMV HA-$Ca_V2.1$, p771; pCMV HA-$Ca_V2.1^{\Delta EF1}$, p939; pCMV HA-$Ca_V1.3$, p1073; pCMV HA-$Ca_V1.3^{2.1Ct}$, p1074; pCMV HA-$Ca_V2.1^{1.3Ct}$, p1075; pCMV HA-$Ca_V1.3^{\mu Ct}$, p1076; pCMV HA-$Ca_V1.3^{2.1ProxCt}$, p1081; pCMV HA-$Ca_V1.3^{2.1DistCt}$, p1082). For these constructs, the Ca_V coding sequences were identical between corresponding pFSW and pCMV versions. The sequence of $Ca_V2.1$ was identical to GenBank Entry AY714490.1 (mouse) with the addition of an HA-tag after position V_{27} flanked by short, exogenous linkers. The resulting cDNAs (p771 and p789) had the sequence M_1ARF … GVVV_{27}-AS-YPYDVPDYA-ACR-G_{28}AAG … DDWC_{2369}. The sequence of $Ca_V1.3$ was as follows: the pore region was identical to residues M_1QHQ … FDYL_{1466} from $Ca_V1.3$e[8a,11,31b,Δ32,42a] (rat) and corresponds to residues M_{10}QHQ … FDYL_{1475} of GenBank Entry EDL89004.1. $Ca_V1.3$e[8a,11,31b,Δ32,42a] was a gift from D. Lipscombe (Addgene Plasmid #49333; http://n2t.net/addgene:49333; RRID:Addgene_49333).[92] The intracellular C-terminal tail was identical to residues T_7 to L_{695} from GenBank Entry AF370010.1 (a partial cDNA, rat); a $Ca_V1.3$ plasmid containing this C-terminal tail was a gift from I. Bezprozvanny.[45] An HA-tag was inserted after position G_{29} (referring to the numbering of Addgene Plasmid #49333) and flanked by short, exogenous linkers. The resulting cDNAs (p1073 and p1077) had the sequence M_1QHQ … SGEG_{29}-AS-YPYDVPDYA-ACR-P_{30}TSQ … FDYL_{1466}-T_{1467}RDW … ITTL_{2155}, with M_1QHQ-SGEG_{29} and P_{30}TSQ-FDYL_{1466} derived from Addgene Plasmid #49333,[92] and with T_{1467}RDW-ITTL_{2155} derived from the plasmid obtained from I. Bezprozvanny.[45] The sequence of $Ca_V^{2.1Ct}$ (p1074 and p1078) contained the pore region (MQHQ … DWSI) from p1077 ($Ca_V1.3$) followed by the C-terminus (LGPH … DDWC) from p789 ($Ca_V2.1$, see Figure S1B). The sequence of $Ca_V2.1^{1.3Ct}$ (p1075 and p1079) contained the pore region (MARF … FEYL) from p789 ($Ca_V2.1$) followed by the C-terminus (TRDW … ITTL) from p1077 ($Ca_V1.3$, see Figure S1B). The sequence of $Ca_V1.3^{2.1ProxCt}$ (p1081 and 1083) contained the pore region (MQHQ … DWSI) from p1077 ($Ca_V1.3$), followed by the proximal C-terminus (LGPH … QAMR) from p789 ($Ca_V2.1$) and then by the distal C-terminus (GKYP … ITTL) from p1077 ($Ca_V1.3$, see Figure S1B). The sequence of

$Ca_V1.3^{2.1DistCt}$ (p1082 and 1084) contained the pore region and the proximal C-terminus (MQHQ … QGLV) from p1077 ($Ca_V1.3$) followed by the distal C-terminus (EEQN … DDWC) from p789 ($Ca_V2.1$, see Figure S1B). In the sequence of $Ca_V2.1^{\Delta EF1}$ (p939 and p947), the first EF hand (EYVR … LRVI) was replaced with residues EY in p789 ($Ca_V2.1$, see Figure S1B). The sequence of $Ca_V1.3^{\Delta Ct}$ (p1076 and 1080) contained the pore region (MQHQ … DWSI) from p1077 ($Ca_V1.3$) and did not contain a C-terminus (see Figure S1B).

Confocal and STED microscopy of synapses—Confocal and STED microscopy and analyses were performed as established before.[20,25,41,58,93,94] Neurons cultured on 0.17 mm thick 12 mm diameter (#1.5) coverslips were washed two times with PBS warmed to 37°C, and then fixed in 2% PFA with 4% sucrose (in PBS) at room temperature. After fixation, coverslips were rinsed three times in PBS with 50 mM glycine, then permeabilized in PBS with 0.1% Triton X-100 and 3% BSA (TBP) for 1 h at room temperature. Coverslips were stained with primary antibodies diluted in TBP for ~48 h at 4°C. The following primary antibodies were used: mouse IgG1 anti-HA (1:500, RRID: AB_2565006, A12), rabbit anti-$Ca_V2.1$ (1:200, RRID: AB_2619841, A46), guinea pig anti-PSD-95 (1:500, RRID: AB_2619800, A5), rabbit anti-synapsin (1:500, RRID: AB_2200097, A30), and mouse IgG1 anti-synapsin (1:500, RRID_2617071, A57). After primary antibody staining, coverslips were rinsed twice and washed three times for 5 min in PBS with 50 mM glycine at room temperature. Alexa Fluor 488 (to detect HA-tagged Ca_Vs or endogenous $Ca_V2.1$; anti-mouse IgG1, RRID: AB_2535764, S7; or, anti-rabbit, RRID: AB_2576217, S5), Alexa Fluor 555 (to detect the postsynaptic marker PSD-95; anti-guinea pig, RRID: AB_2535856, S23), and Alexa Fluor 633 (to detect the synaptic vesicle cluster; anti-rabbit, RRID: AB_2535731, S33; or, anti-mouse IgG1, RRID: AB_2535768, S29) conjugated antibodies were diluted in TBP at 1:200 (for Alexa Fluor 488 and 555) or 1:500 (for Alexa Fluor 633), and coverslips were incubated with the secondary antibody solution for ~24 h at 4°C. Coverslips were then rinsed twice with PBS with 50 mM glycine and once with deionized water, air-dried and mounted on glass slides in fluorescent mounting medium. Confocal and STED images were acquired on a Leica SP8 Confocal/STED 3X microscope with a 100x oil-immersion 1.44 numerical aperture objective and gated detectors as established before.[20,93] 58.14 x 58.14 μm^2 areas were acquired using 2x digital zoom (4096 x 4096 $pixel^2$, pixel size of 14.194 × 14.194 nm^2). Alexa Fluor 633, Alexa Fluor 555, and Alexa Fluor 488 were excited at 633 nm, 555 nm and 488 nm using a white light laser at 1–10% of 1.5 mW laser power. The Alexa Fluor 633, Alexa Fluor 555, and Alexa Fluor 488 channels were acquired first in confocal mode. For the Alexa Fluor 555 and Alexa Fluor 488 channels, the same areas were then sequentially acquired in STED mode using 660 nm and 592 nm depletion lasers, respectively. Identical imaging and laser settings were applied to all conditions within a given biological repeat. For analyses of presynaptic Ca_V distribution in STED images, synapses were selected in side-view. Side-view synapses were defined as synapses that contained a synaptic vesicle cluster labeled with synapsin and were associated with an elongated PSD-95 structure along the edge of the vesicle cluster as established before.[20,41,57,93,95] For intensity profile analyses, a ~1000 nm long, 200 nm wide, rectangular ROI was drawn perpendicular and across the center of the PSD-95 structure, and the intensity profiles were obtained using this ROI for both the protein of

interest and PSD-95. To align individual profiles, the PSD-95 signal only was smoothened using a rolling average of 5 pixels, and the smoothened signal was used to define the peak position of PSD-95. The profiles for the protein of interest (Ca_V or HA) and smoothened PSD-95 were aligned to the PSD-95 peak position, averaged across synapses, and then plotted. Peak intensities were also analyzed by extracting the maximal value from the line profiles of the protein of interest (Ca_V or HA) and smoothened PSD-95 within a 200 nm window around the PSD-95 peak. Peak intensity values were plotted for each synapse and averaged. For quantification of confocal images, a custom MATLAB program (https://doi.org/10.5281/zenodo.6388196) was used to generate masks of the presynaptic marker (synapsin), with the threshold determined by automatic two-dimensional segmentation (Otsu algorithm).[91,95] Regions of interest (ROIs) were defined as synapsin-positive areas formed by contiguous pixels of at least 0.05 μm^2 in size. Each image typically contained between 500 and 1500 synapsin ROIs. Levels of HA or $Ca_V2.1$ within these ROIs were measured and the average intensity across all ROIs within an image was calculated and plotted. Representative images in figures were cropped, rotated with bi-linear interpolation, and then brightness and contrast adjusted to facilitate inspection. Brightness and contrast adjustments were made for display in figures and were done identically for images within an experiment, but image quantification was performed on raw images without these adjustments. The experimenter was blind to the condition/genotype for image acquisition and analyses for STED and confocal microscopic experiments.

Confocal imaging of neuronal somata—Neurons cultured on 0.17 mm thick 12 mm diameter (#1.5) coverslips were washed with PBS warmed to 37°C and fixed in 2% PFA with 4% sucrose for 10 min at room temperature. Coverslips were then rinsed three times in PBS with 50 mM glycine at room temperature, permeabilized in TBP for 1 h at room temperature, and incubated in primary antibodies for ~48 h at 4°C. The following primary antibodies were used: mouse IgG1 anti-HA (1:500, RRID: AB_2565006, A12) and mouse IgG2b anti-NeuN (1:500, RRID: AB_10711040, A254). After staining with primary antibodies, coverslips were rinsed twice and washed three times for 5 min in PBS with 50 mM glycine at room temperature. Alexa Fluor 555 (to detect HA; anti-mouse IgG1, RRID: AB_2535769, S19), and 633 (to detect neuronal somata; anti-mouse IgG2b, RRID: AB_1500899, S31) conjugated secondary antibodies were used at 1:500 dilution in TBP. Secondary antibody staining was carried out for ~24 h at 4°C. Coverslips were rinsed twice in PBS with 50 mM glycine and once in deionized water, then air-dried and mounted on glass slides using fluorescent mounting medium. Confocal images of neuronal somata were acquired on a Leica Stellaris 5 microscope with a 63x oil-immersion objective. Single section, 92.65 x 92.65 μm^2 areas were acquired using 2x digital zoom (1024 x 1024 $pixel^2$, pixel size of 90.2 x 90.2 nm^2). Imaging and laser settings were identical for all conditions within a given biological repeat. For analyses of somatic HA signals, the NeuN signal was used to mark the neuron somata, and EGFP-Cre or EGFP-ΔCre was used to define nuclei. Somatic ROIs were drawn as donut shapes by using the outer edge of the NeuN profile along the main somatic compartment not including neurites, and by excluding the EGFP-labeled nucleus. The average pixel intensity within the somatic ROI was then calculated for the HA channel and plotted for each cell. Representative images in figures were cropped and adjusted for brightness and contrast to facilitate inspection. Brightness and

contrast adjustments were made for display in figures and were done identically for images within an experiment, but image quantification was performed on raw images without these adjustments. The experimenter was blind to the condition/genotype for image acquisition and analyses.

Electrophysiological recordings from neurons—Electrophysiological recordings in cultured hippocampal neurons were performed as established before[20,41,95] at DIV16 to 19. Glass pipettes were pulled at 2 to 5 MΩ and filled with intracellular solution containing (in mM) for mEPSCs and EPSCs: 120 Cs-methane-sulfonate, 2 $MgCl_2$, 10 EGTA, 4 Na_2-ATP, 1 Na-GTP, 4 QX314-Cl, 10 HEPES-CsOH (pH 7.4, ~300 mOsm); and for mIPSCs and IPSCs: 40 CsCl, 90 K-gluconate, 1.8 NaCl, 1.7 $MgCl_2$, 3.5 KCl, 0.05 EGTA, 2 Mg-ATP, 0.4 Na_2-GTP, 10 phosphocreatine, 4 QX314-Cl, 10 HEPES-CsOH (pH 7.2, ~300 mOsm). The extracellular solution contained (in mM): 140 NaCl, 5 KCl, 2 $MgCl_2$, 1.5 $CaCl_2$, 10 glucose, 10 HEPES-NaOH (pH 7.4, −300 mOsm). Cells were held at +40 mV for NMDAR-EPSCs and at −70 mV for IPSCs, mIPSCs, and mEPSCs, and recordings were performed at room temperature (20°C–24°C). For recording of evoked synaptic currents, access resistance was compensated to 2–3 MΩ, and cells were discarded if the uncompensated access resistance exceeded 15 MΩ. For recordings of miniature synaptic currents, cells were discarded if the uncompensated access resistance exceeded 20 MΩ. The following drugs were added to the extracellular solution: for NMDAR-EPSCs, picrotoxin (PTX, 50 μM) and 6-Cyano-7-nitroquinoxaline-2,3-dione (CNQX, 20 μM); for IPSCs, D-2-amino-5-phosphonopentanoic acid (D-AP5, 50 μM) and CNQX (20 μM); for mEPSCs, TTX (1 μM), PTX (50 μM), and D-AP5 (50 μM); and for mIPSCs, TTX (1 μM), D-AP5 (50 μM), and CNQX (20 μM). Action potentials were elicited with a bipolar focal stimulation electrode fabricated from nichrome wire. To evaluate the Ca_V blocker sensitivity of synaptic transmission, ω-agatoxin IVA (to block $Ca_V2.1$) or isradipine (to block Ca_V1s) were used. Blockers were pipetted into the recording chamber as stocks diluted in extracellular solution for a final working concentration of 200 nM ω-agatoxin IVA and 20 μM isradipine. For wash-in, cells were incubated after blocker addition for 5 min. IPSCs were recorded first in the absence of Ca_V blockers. Then, IPSCs were measured after wash-in of 200 nM ω-agatoxin IVA and again after wash-in of 200 nM ω-agatoxin IVA and 20 μM isradipine (Figures 4F-4I), or after wash-in of 20 μM isradipine (Figures S4H-S4J). Data were acquired at 10 kHz and lowpass filtered at 2 kHz with an Axon 700B Multiclamp amplifier and digitized with a Digidata 1440A digitizer. Data acquisition and analyses were done using pClamp10. Spontaneous mEPSCs and mIPSCs were identified with a template search and individually cross-checked. Frequencies were obtained for each cell by dividing the event count by the recording duration, and amplitudes were quantified per cell by extracting the peak amplitude of each event followed by averaging. For electrophysiological experiments, the experimenter was blind to the genotype throughout data acquisition and analyses.

Western blotting—Lysates from transfected HEK293T cells were used for Western blotting. Ca_V1 and Ca_V2 constructs were co-transfected with $Ca_V\beta1b$ (p754; pMT2 $Ca_V\beta1b$-GFP was a gift from A. Dolphin, Addgene plasmid # 89893; http://n2t.net/addgene:89893; RRID: Addgene_89893)[36] and $Ca_V\alpha2\delta1$ (p752; $Ca_V\alpha2\delta1$ was a gift from D. Lipscombe, Addgene plasmid # 26575; http://n2t.net/ addgene:26575; RRID:

Addgene_26575).[84] Plasmids were transfected with the Ca^{2+} phosphate method at a 1:1:1 molar ratio with a total of 6.7 μg of DNA. Around 48 h after transfection, HEK293T cells were harvested in 1 mL of standard 1x SDS buffer per flask. Homogenates were centrifuged at 16,200 x g for 10 min at room temperature, run on 6% (for Ca_Vs) or 12% (for β-actin) polyacrylamide gels, and transferred onto nitrocellulose membranes for 6.5 h at 4°C in transfer buffer (containing per L, 200 mL methanol, 14 g glycine, 3 g Tris). Membranes were blocked in filtered 10% nonfat milk/5% goat serum in TBST (Tris-buffered saline with 0.1% Tween) for 1 h at room temperature and incubated with primary antibodies in 5% nonfat milk/2.5% goat serum in TBST overnight at 4°C. The primary antibodies used were mouse IgG1 anti-HA (1:1000; RRID: AB_2565006, A12) and mouse IgG1 anti-β-actin (1:2000; RRID: AB_476692, A127). Membranes were washed five times for 3 min each at room temperature in TBST and then incubated with secondary antibodies in 5% nonfat milk/2.5% goat serum in TBST for 1 h at room temperature. The secondary antibodies used were peroxidase-conjugated goat anti-mouse IgG (1:10,000, RRID: AB_2334540, S52) and peroxidase-conjugated goat anti-rabbit IgG (1:10,000, RRID: AB_2334589, S53). Membranes were again washed five times for 3 min each at room temperature in TBST, then incubated in a chemiluminescent reagent for 30 s. Finally, the membranes were exposed to films, and films were developed and scanned. Corresponding western blots of Ca_Vs and β-actin were run simultaneously, on the same day, and on separate gels using the same samples. For illustration in figures, blots were rotated with bilinear interpolation and cropped for display.

Electrophysiological recordings in HEK293T cells—Electrophysiological recordings in HEK293T cells were performed as established before.[20] HEK293T cells plated on 12 mm diameter coverslips were transfected by the Ca^{2+} phosphate method with Ca_Vβ1 (p754), Ca_Vα2Δ1 (p752), and a Ca_Vα1 subunit. Constructs were transfected at a 1:1:1 molar ratio with a total of 1 mg of DNA per coverslip. Current recordings were carried out 48 h after transfection at room temperature (20°C–24°C). The extracellular solution contained (in mM): 10 $BaCl_2$, 140 TEA-Cl, 10 HEPES, and 10 glucose (7.4 pH with TEA-OH). Glass pipettes were pulled at 2 to 5 MU and filled with intracellular solution containing (in mM): 135 Cs-methanesulfonate, 5 CsCl, 0.5 EGTA, 5 $MgCl_2$, 4 Na_2-ATP, and 10 HEPES (pH7.2 with CsOH). Whole cell recordings were performed on HEK293T cells with robust GFP expression, and cells were discarded if the access resistance exceeded 15 MΩ. To characterize the current-voltage relationship, cells were held at −80 mV, and inward currents were evoked by 50 ms depolarizations from −70 mV to +50 mV in increments of 10 mV. The maximal current during each depolarization step was normalized to the overall peak inward current to generate a normalized I-V curve. Only cells that had a peak inward current greater than 300 pA at any voltage step were included in the analysis. Data were acquired with an Axon 700B Multiclamp amplifier and digitized with a Digidata 1440A digitizer. Pulse-noise leak subtraction was used to isolate active currents, and no resistance compensation was applied. The experimenter was blind to the genotype throughout data acquisition and analyses.

QUANTIFICATION AND STATISTICAL ANALYSES

Data are displayed as mean ± SEM. Individual data points are displayed as open circles for datasets with sample sizes below 100. Violin plots were used for datasets with sample sizes above 100. Statistics were performed in GraphPad Prism 9, and significance is presented as $*p < 0.05$, $**p < 0.01$, and $***p < 0.001$. Sample sizes and statistical tests for each experiment are included in each figure legend. For electrophysiological experiments, the sample size used for statistical analyses was the number of recorded cells. For STED microscopic data, the sample size used for statistical analyses was the number of synapses. For confocal microscopic data, the sample size used for statistical analyses was the number of images for analyses of synapsin ROIs, or the number of neurons for analyses of somata. Non-parametric tests that do not make assumptions of data normality and homoscedasticity were used whenever possible to compare genotypes or experimental conditions. Single factor, multiple group comparisons were conducted using Kruskal-Wallis tests followed by Dunn's multiple comparisons post-hoc tests for proteins of interest (HA or $Ca_V2.1$), for current amplitudes (EPSCs, IPSCs), and for event frequencies (mEPSCs, mIPSCs). To compare the efficacy of blockade of synaptic transmission by different pharmacological agents in Figure 4H, Friedman tests and Dunn's multiple comparisons post-hoc tests were used. To compare the effects of Ca_V blockers on synaptic transmission across genotypes in Figures 4I, a two-way, repeated-measures ANOVA and Dunnett's multiple comparisons post-hoc tests was used. To compare the current-voltage relationship for multiple Ca_V constructs in Figure S4C, a two-way, repeated-measures ANOVA was used. To assess blocker sensitivity in Figure S4J, the Wilcoxon matched-pairs signed rank test was used.

Supplementary Material

Refer to Web version on PubMed Central for supplementary material.

ACKNOWLEDGMENTS

We thank members of the Kaeser laboratory for insightful discussions and comments. We specifically acknowledge R. Held, H. Nyitrai, C. Tan, K. Ma, and A. Morabito for help and advice early in the project and/or feedback on the findings and the manuscript. We acknowledge J. Wang, C. Qiao, V. Charles, and G. Handy for technical support. We thank A.M.J.M. van den Maagdenberg for providing $Ca_V2.1$ floxed mice and T. Schneider for $Ca_V2.3$ floxed mice. This work was supported by the NIH (R01NS083898 to P.S.K. and F31NS127399 to M.C.), a Stuart H.Q. and Victoria Quan fellowship (to M.C.), and Harvard Medical School. We acknowledge the Neurobiology Imaging Facility at Harvard Medical School for microscope availability and support.

REFERENCES

1. y Cajal SR, and Sherrington SCS (1891). Significación fisiológica de las expansiones protoplasmáticas y nerviosas de las células de la sustancia gris (Establecimento tipografico).
2. Bentley M, and Banker G (2016). The cellular mechanisms that maintain neuronal polarity. Nat. Rev. Neurosci 17, 611–622. 10.1038/NRN.2016.100. [PubMed: 27511065]
3. Rizalar FS, Roosen DA, and Haucke V (2021). A Presynaptic Perspective on Transport and Assembly Mechanisms for Synapse Formation. Neuron 109, 27–41. 10.1016/j.neuron.2020.09.038. [PubMed: 33098763]
4. Catterall WA (2011). Voltage-Gated Calcium Channels. Cold Spring Harbor Perspect. Biol. 3, a003947. 10.1101/cshperspect.a003947.
5. Simms BA, and Zamponi GW (2014). Neuronal voltage-gated calcium channels: Structure, function, and dysfunction. Neuron 82, 24–45. 10.1016/j.neuron.2014.03.016. [PubMed: 24698266]

6. Dolphin AC (2012). Calcium channel auxiliary α2δ and β subunits: trafficking and one step beyond. Nat. Rev. Neurosci 13, 542–555. 10.1038/nrn3311. [PubMed: 22805911]
7. Catterall WA, Perez-Reyes E, Snutch TP, and Striessnig J (2005). International Union of Pharmacology. XLVIII. Nomenclature and structure-function relationships of voltage-gated calcium channels. Pharmacol. Rev 57, 411–425. 10.1124/pr.57.4.5. [PubMed: 16382099]
8. Greer PL, and Greenberg ME (2008). From Synapse to Nucleus: Calcium-Dependent Gene Transcription in the Control of Synapse Development and Function. Neuron 59, 846–860. 10.1016/j.neuron.2008.09.002. [PubMed: 18817726]
9. Bading H, Ginty DD, and Greenberg ME (1993). Regulation of gene expression in hippocampal neurons by distinct calcium signaling pathways. Science 260, 181–186. 10.1126/SCIENCE.8097060. [PubMed: 8097060]
10. Dolmetsch RE, Pajvani U, Fife K, Spotts JM, and Greenberg ME (2001). Signaling to the nucleus by an L-type calcium channel-calmodulin complex through the MAP kinase pathway. Science 294, 333–339. 10.1126/SCIENCE.1063395. [PubMed: 11598293]
11. Bito H, Deisseroth K, and Tsien RW (1996). CREB phosphorylation and dephosphorylation: a Ca(2+)- and stimulus duration-dependent switch for hippocampal gene expression. Cell 87, 1203–1214. 10.1016/S0092-8674(00)81816-4. [PubMed: 8980227]
12. Liu Y, Harding M, Pittman A, Dore J, Striessnig J, Rajadhyaksha A, and Chen X (2014). Cav1.2 and Cav1.3 L-type calcium channels regulate dopaminergic firing activity in the mouse ventral tegmental area. J. Neurophysiol 112, 1119–1130. 10.1152/JN.00757.2013. [PubMed: 24848473]
13. Chan CS, Guzman JN, Ilijic E, Mercer JN, Rick C, Tkatch T, Meredith GE, and Surmeier DJ (2007). "Rejuvenation" protects neurons in mouse models of Parkinson's disease. Nature 447, 1081–1086. 10.1038/nature05865. [PubMed: 17558391]
14. Putzier I, Kullmann PHM, Horn JP, and Levitan ES (2009). Cav1.3 channel voltage dependence, not Ca2+ selectivity, drives pacemaker activity and amplifies bursts in nigral dopamine neurons. J. Neurosci 29, 15414–15419. 10.1523/JNEUROSCI.4742-09.2009. [PubMed: 20007466]
15. Jackson AC, Yao GL, and Bean BP (2004). Mechanism of spontaneous firing in dorsomedial suprachiasmatic nucleus neurons. J. Neurosci 24, 7985–7998. 10.1523/JNEUROSCI.2146-04.2004. [PubMed: 15371499]
16. Berkefeld H, Sailer CA, Bildl W, Rohde V, Thumfart JO, Eble S, Klugbauer N, Reisinger E, Bischofberger J, Oliver D, et al. (2006). BKCa-Cav channel complexes mediate rapid and localized Ca2+-activated K+ signaling. Science 314, 615–620. 10.1126/SCIENCE.1132915. [PubMed: 17068255]
17. Takahashi T, and Momiyama A (1993). Different types of calcium channels mediate central synaptic transmission. Nature 366, 156–158. 10.1038/366156a0. [PubMed: 7901765]
18. Poncer JC, McKinney RA, Gähwiler BH, and Thompson SM (1997). Either N- or P-type calcium channels mediate GABA release at distinct hippocampal inhibitory synapses. Neuron 18, 463–472. 10.1016/S0896-6273(00)81246-5. [PubMed: 9115739]
19. Regehr WG, and Mintz IM (1994). Participation of multiple calcium channel types in transmission at single climbing fiber to Purkinje cell synapses. Neuron 12, 605–613. 10.1016/0896-6273(94)90216-x. [PubMed: 8155322]
20. Held RG, Liu C, Ma K, Ramsey AM, Tarr TB, De Nola G, Wang SSH, Wang J, van den Maagdenberg AMJM, Schneider T, et al. (2020). Synapse and Active Zone Assembly in the Absence of Presynaptic Ca2+ Channels and Ca2+ Entry. Neuron 107, 667–683.e9. 10.1016/j.neuron.2020.05.032. [PubMed: 32616470]
21. Nakamura Y, Harada H, Kamasawa N, Matsui K, Rothman JS, Shigemoto R, Silver RA, DiGregorio DA, and Takahashi T (2015). Nanoscale Distribution of Presynaptic Ca2+ Channels and Its Impact on Vesicular Release during Development. Neuron 85, 145–158. 10.1016/j.neuron.2014.11.019. [PubMed: 25533484]
22. Bucurenciu I, Kulik A, Schwaller B, Frotscher M, and Jonas P (2008). Nanodomain coupling between Ca2+ channels and Ca2+ sensors promotes fast and efficient transmitter release at a cortical GABAergic synapse. Neuron 57, 536–545. 10.1016/j.neuron.2007.12.026. [PubMed: 18304483]

23. Han Y, Kaeser PS, Südhof TC, and Schneggenburger R (2011). RIM determines Ca^{2+} channel density and vesicle docking at the presynaptic active zone. Neuron 69, 304–316. 10.1016/j.neuron.2010.12.014. [PubMed: 21262468]
24. Kaeser PS, Deng L, Wang Y, Dulubova I, Liu X, Rizo J, and Südhof TC (2011). RIM proteins tether Ca2+ channels to presynaptic active zones via a direct PDZ-domain interaction. Cell 144, 282–295. 10.1016/j.cell.2010.12.029. [PubMed: 21241895]
25. Emperador-Melero J, Andersen JW, Metzbower SR, Levy AD, Dharmasri PA, de Nola G, Blanpied TA, Kaeser PS (2023). Distinct active zone protein machineries mediate Ca^{2+} channel clustering and vesicle priming at hippocampal synapses. Nat. Neuroscience in press. 10.1101/2023.10.27.564439.
26. Dolphin AC, and Lee A (2020). Presynaptic calcium channels: specialized control of synaptic neurotransmitter release. Nat. Rev. Neurosci 21, 213–229. 10.1038/s41583-020-0278-2. [PubMed: 32161339]
27. Gao S, Yao X, and Yan N (2021). Structure of human Cav2.2 channel blocked by the painkiller ziconotide. Nature 596, 143–147. 10.1038/s41586-021-03699-6. [PubMed: 34234349]
28. Wu J, Yan Z, Li Z, Qian X, Lu S, Dong M, Zhou Q, and Yan N (2016). Structure of the voltage-gated calcium channel Ca(v)1.1 at 3.6 Å resolution. Nature 537, 191–196. 10.1038/nature19321. [PubMed: 27580036]
29. Bichet D, Cornet V, Geib S, Carlier E, Volsen S, Hoshi T, Mori Y, and De Waard M (2000). The I-II loop of the Ca2+ channel alpha1 subunit contains an endoplasmic reticulum retention signal antagonized by the beta subunit. Neuron 25, 177–190. 10.1016/S0896-6273(00)80881-8. [PubMed: 10707982]
30. Fang K, and Colecraft HM (2011). Mechanism of auxiliary β-subunit-mediated membrane targeting of L-type (Ca(V)1.2) channels. J. Physiol 589, 4437–4455. 10.1113/JPHYSIOL.2011.214247. [PubMed: 21746784]
31. Altier C, Garcia-Caballero A, Simms B, You H, Chen L, Walcher J, Tedford HW, Hermosilla T, and Zamponi GW (2011). The Cavβ subunit prevents RFP2-mediated ubiquitination and proteasomal degradation of L-type channels. Nat. Neurosci 14, 173–180. 10.1038/NN.2712. [PubMed: 21186355]
32. Hoppa MB, Lana B, Margas W, Dolphin AC, and Ryan TA (2012). α2δ expression sets presynaptic calcium channel abundance and release probability. Nature 486, 122–125. 10.1038/nature11033. [PubMed: 22678293]
33. Wang HG, George MS, Kim J, Wang C, and Pitt GS (2007). Ca2+/calmodulin regulates trafficking of Ca(V)1.2 Ca2+ channels in cultured hippocampal neurons. J. Neurosci 27, 9086–9093. 10.1523/JNEUROSCI.1720-07.2007. [PubMed: 17715345]
34. Hall DD, Dai S, Tseng PY, Malik Z, Nguyen M, Matt L, Schnizler K, Shephard A, Mohapatra DP, Tsuruta F, et al. (2013). Competition between α-actinin and Ca^{2+}-calmodulin controls surface retention of the L-type Ca^{2+} channel Ca(V)1.2. Neuron 78, 483–497. 10.1016/J.NEURON.2013.02.032. [PubMed: 23664615]
35. Waithe D, Ferron L, Page KM, Chaggar K, and Dolphin AC (2011). Beta-subunits promote the expression of Ca(V)2.2 channels by reducing their proteasomal degradation. J. Biol. Chem 286, 9598–9611. 10.1074/JBC.M110.195909. [PubMed: 21233207]
36. Page KM, Rothwell SW, and Dolphin AC (2016). The CaVβ Subunit Protects the I-II Loop of the Voltage-gated Calcium Channel CaV2.2 from Proteasomal Degradation but Not Oligoubiquitination. J. Biol. Chem 291, 20402–20416. 10.1074/jbc.M116.737270. [PubMed: 27489103]
37. Hibino H, Pironkova R, Onwumere O, Vologodskaia M, Hudspeth AJ, and Lesage F (2002). RIM binding proteins (RBPs) couple Rab3-interacting molecules (RIMs) to voltage-gated Ca(2+) channels. Neuron 34, 411–423. 10.1016/S0896-6273(02)00667-0. [PubMed: 11988172]
38. Wu X, Cai Q, Shen Z, Chen X, Zeng M, Du S, and Zhang M (2019). RIM and RIM-BP Form Presynaptic Active-Zone-like Condensates via Phase Separation. Mol. Cell 73, 971–984.e5. 10.1016/j.molcel.2018.12.007. [PubMed: 30661983]

39. Acuna C, Liu X, and Südhof TC (2016). How to Make an Active Zone: Unexpected Universal Functional Redundancy between RIMs and RIM-BPs. Neuron 91, 792–807. 10.1016/j.neuron.2016.07.042. [PubMed: 27537484]
40. Wang SSH, Held RG, Wong MY, Liu C, Karakhanyan A, and Kaeser PS (2016). Fusion Competent Synaptic Vesicles Persist upon Active Zone Disruption and Loss of Vesicle Docking. Neuron 91, 777–791. 10.1016/j.neuron.2016.07.005. [PubMed: 27537483]
41. Tan C, Wang SSH, de Nola G, and Kaeser PS (2022). Rebuilding essential active zone functions within a synapse. Neuron 110, 1498–1515.e8. 10.1016/j.neuron.2022.01.026. [PubMed: 35176221]
42. Kushibiki Y, Suzuki T, Jin Y, and Taru H (2019). RIMB-1/RIM-Binding Protein and UNC-10/RIM Redundantly Regulate Presynaptic Localization of the Voltage-Gated Calcium Channel in Caenorhabditis elegans. J. Neurosci 39, 8617–8631. 10.1523/JNEUROSCI.0506-19.2019. [PubMed: 31530643]
43. Oh KH, Krout MD, Richmond JE, and Kim H (2021). UNC-2 CaV2 Channel Localization at Presynaptic Active Zones Depends on UNC-10/RIM and SYD-2/Liprin-α in Caenorhabditis elegans. J. Neurosci 41, 4782–4794. 10.1523/JNEUROSCI.0076-21.2021. [PubMed: 33975919]
44. Maximov A, and Bezprozvanny I (2002). Synaptic targeting of N-type calcium channels in hippocampal neurons. J. Neurosci 22, 6939–6952. 10.1523/JNEUROSCI.22-16-06939.2002. [PubMed: 12177192]
45. Zhang H, Maximov A, Fu Y, Xu F, Tang TS, Tkatch T, Surmeier DJ, and Bezprozvanny I (2005). Association of CaV1.3 L-type calcium channels with Shank. J. Neurosci 25, 1037–1049. 10.1523/JNEUROSCI.4554-04.2005. [PubMed: 15689539]
46. Gao T, Bunemann M, Gerhardstein BL, Ma H, and Hosey MM (2000). Role of the C terminus of the alpha 1C (CaV1.2) subunit in membrane targeting of cardiac L-type calcium channels. J. Biol. Chem 275, 25436–25444. 10.1074/JBC.M003465200. [PubMed: 10816591]
47. Lübbert M, Goral RO, Satterfield R, Putzke T, van den Maagdenberg AM, Kamasawa N, and Young SM (2017). A novel region in the CaV2.1 α1 subunit C-terminus regulates fast synaptic vesicle fusion and vesicle docking at the mammalian presynaptic active zone. Elife 6, e28412. 10.7554/eLife.28412. [PubMed: 28786379]
48. Li J, Veeraraghavan P, and Young SM (2024). CaV 2.1 α1 subunit motifs that control presynaptic CaV 2.1 subtype abundance are distinct from CaV 2.1 preference. J. Physiol 602, 485–506. 10.1113/JP284957. [PubMed: 38155373]
49. Sheng ZH, Rettig J, Takahashi M, and Catterall WA (1994). Identification of a syntaxin-binding site on N-type calcium channels. Neuron 13, 1303–1313. 10.1016/0896-6273(94)90417-0. [PubMed: 7993624]
50. Sheng ZH, Rettig J, Cook T, and Catterall WA (1996). Calcium-dependent interaction of N-type calcium channels with the synaptic core complex. Nature 379, 451–454. 10.1038/379451a0. [PubMed: 8559250]
51. Rettig J, Heinemann C, Ashery U, Sheng ZH, Yokoyama CT, Catterall WA, and Neher E (1997). Alteration of Ca2+ dependence of neurotransmitter release by disruption of Ca2+ channel/syntaxin interaction. J. Neurosci 17, 6647–6656. 10.1523/JNEUROSCI.17-17-06647.1997. [PubMed: 9254677]
52. Szabo Z, Obermair GJ, Cooper CB, Zamponi GW, and Flucher BE, (2006). Role of the synprint site in presynaptic targeting of the calcium channel CaV2.2 in hippocampal neurons. Eur. J. Neurosci 24, 709–718. 10.1111/J.1460-9568.2006.04947.X. [PubMed: 16930401]
53. Spafford JD, Munno DW, Van Nierop P, Feng Z-P, Jarvis SE, Gallin WJ, Smit AB, Zamponi GW, and Syed NI (2003). Calcium channel structural determinants of synaptic transmission between identified invertebrate neurons. J. Biol. Chem 278, 4258–4267. 10.1074/jbc.M211076200. [PubMed: 12458203]
54. Nishimune H, Sanes JR, and Carlson SS (2004). A synaptic laminin-calcium channel interaction organizes active zones in motor nerve terminals. Nature 432, 580–587. 10.1038/nature03112. [PubMed: 15577901]

55. Chen J, Billings SE, and Nishimune H (2011). Calcium channels link the muscle-derived synapse organizer laminin β2 to Bassoon and CAST/Erc2 to organize presynaptic active zones. J. Neurosci 31, 512–525. 10.1523/JNEUROSCI.3771-10.2011. [PubMed: 21228161]
56. Mark MD, Maejima T, Kuckelsberg D, Yoo JW, Hyde RA, Shah V, Gutierrez D, Moreno RL, Kruse W, Noebels JL, and Herlitze S (2011). Delayed Postnatal Loss of P/Q-Type Calcium Channels Recapitulates the Absence Epilepsy, Dyskinesia, and Ataxia Phenotypes of Genomic Cacna1A Mutations. J. Neurosci 31, 4311–4326. 10.1523/JNEUROSCI.5342-10.2011. [PubMed: 21411672]
57. Nyitrai H, Wang SSH, and Kaeser PS (2020). ELKS1 Captures Rab6-Marked Vesicular Cargo in Presynaptic Nerve Terminals. Cell Rep. 31, 107712. 10.1016/j.celrep.2020.107712. [PubMed: 32521280]
58. Emperador-Melero J, Wong MY, Wang SSH, de Nola G, Nyitrai H, Kirchhausen T, and Kaeser PS (2021). PKC-phosphorylation of Liprin-α3 triggers phase separation and controls presynaptic active zone structure. Nat. Commun 12, 3057. 10.1038/s41467-021-23116-w. [PubMed: 34031393]
59. Babitch J. (1990). Channel hands. Nature 346, 321–322. 10.1038/346321B0. [PubMed: 2165218]
60. Ben Johny M, Yang PS, Bazzazi H, and Yue DT (2013). Dynamic switching of calmodulin interactions underlies Ca2+ regulation of CaV1.3 channels. Nat. Commun 4, 1717. 10.1038/ncomms2727. [PubMed: 23591884]
61. Chaudhuri D, Chang SY, DeMaria CD, Alvania RS, Soong TW, and Yue DT (2004). Alternative splicing as a molecular switch for Ca2+/calmodulin-dependent facilitation of P/Q-type Ca2+ channels. J. Neurosci 24, 6334–6342. 10.1523/JNEUROSCI.1712-04.2004. [PubMed: 15254089]
62. Peterson BZ, Lee JS, Mulle JG, Wang Y, De Leon M, and Yue DT (2000). Critical determinants of Ca(2+)-dependent inactivation within an EF-hand motif of L-type Ca(2+) channels. Biophys. J 78, 1906–1920. 10.1016/S0006-3495(00)76739-7. [PubMed: 10733970]
63. Barrett CF, Cao YQ, and Tsien RW (2005). Gating deficiency in a familial hemiplegic migraine type 1 mutant P/Q-type calcium channel. J. Biol. Chem 280, 24064–24071. 10.1074/jbc.M502223200. [PubMed: 15795222]
64. Gumy LF, and Hoogenraad CC (2018). Local mechanisms regulating selective cargo entry and long-range trafficking in axons. Curr. Opin. Neurobiol 51, 23–28. 10.1016/J.CONB.2018.02.007. [PubMed: 29510294]
65. Maeder CI, Shen K, and Hoogenraad CC (2014). Axon and dendritic trafficking. Curr. Opin. Neurobiol 27, 165–170. 10.1016/J.CONB.2014.03.015. [PubMed: 24762653]
66. Emperador-Melero J, and Kaeser PS (2020). Assembly of the presynaptic active zone. Curr. Opin. Neurobiol 63, 95–103. 10.1016/j.conb.2020.03.008. [PubMed: 32403081]
67. Ben-Johny M, Yang PS, Niu J, Yang W, Joshi-Mukherjee R, and Yue DT (2014). Conservation of Ca2+/calmodulin regulation across Na and Ca2+ channels. Cell 157, 1657–1670. 10.1016/J.CELL.2014.04.035. [PubMed: 24949975]
68. Macabuag N, and Dolphin AC (2015). Alternative Splicing in CaV2.2 Regulates Neuronal Trafficking via Adaptor Protein Complex-1 Adaptor Protein Motifs. J. Neurosci 35, 14636–14652. 10.1523/JNEUROSCI.3034-15.2015. [PubMed: 26511252]
69. Meyer JO, Dahimene S, Page KM, Ferron L, Kadurin I, Ellaway JIJ, Zhao P, Patel T, Rothwell SW, Lin P, et al. (2019). Disruption of the Key Ca2+ Binding Site in the Selectivity Filter of Neuronal Voltage-Gated Calcium Channels Inhibits Channel Trafficking. Cell Rep. 29, 22–33.e5. 10.1016/j.celrep.2019.08.079. [PubMed: 31577951]
70. Cao Y-Q, Piedras-Rentería ES, Smith GB, Chen G, Harata NC, and Tsien RW (2004). Presynaptic Ca2+ channels compete for channel type-preferring slots in altered neurotransmission arising from Ca2+ channelopathy. Neuron 43, 387–400. 10.1016/j.neuron.2004.07.014. [PubMed: 15294146]
71. Cao YQ, and Tsien RW (2010). Different relationship of N- and P/Q-type Ca2+ channels to channel-interacting slots in controlling neurotransmission at cultured hippocampal synapses. J. Neurosci 30, 4536–4546. 10.1523/JNEUROSCI.5161-09.2010. [PubMed: 20357104]
72. Soong TW, DeMaria CD, Alvania RS, Zweifel LS, Liang MC, Mittman S, Agnew WS, and Yue DT (2002). Systematic identification of splice variants in human P/Q-type channel alpha1(2.1)

subunits: implications for current density and Ca2+-dependent inactivation. J. Neurosci 22, 10142–10152. 10.1523/JNEUROSCI.22-23-10142.2002. [PubMed: 12451115]

73. Castiglioni AJ, Raingo J, and Lipscombe D (2006). Alternative splicing in the C-terminus of CaV2.2 controls expression and gating of N-type calcium channels. J. Physiol 576, 119–134. 10.1113/JPHYSIOL.2006.115030. [PubMed: 16857708]
74. Breustedt J, Vogt KE, Miller RJ, Nicoll RA, and Schmitz D (2003). Alpha1E-containing Ca2+ channels are involved in synaptic plasticity. Proc. Natl. Acad. Sci. USA 100, 12450–12455. 10.1073/pnas.2035117100. [PubMed: 14519849]
75. Dietrich D, Kirschstein T, Kukley M, Pereverzev A, von der Brelie C, Schneider T, and Beck H (2003). Functional Specialization of Presynaptic Cav2.3 Ca2+ Channels. Neuron 39, 483–496. 10.1016/S0896-6273(03)00430-6. [PubMed: 12895422]
76. Goswami SP, Bucurenciu I, and Jonas P (2012). Miniature IPSCs in hippocampal granule cells are triggered by voltage-gated Ca2+ channels via microdomain coupling. J. Neurosci 32, 14294–14304. 10.1523/JNEUROSCI.6104-11.2012. [PubMed: 23055500]
77. Ermolyuk YS, Alder FG, Surges R, Pavlov IY, Timofeeva Y, Kullmann DM, and Volynski KE (2013). Differential triggering of spontaneous glutamate release by P/Q-N- and R-type Ca2+ channels. Nat. Neurosci 16, 1754–1763. 10.1038/NN.3563. [PubMed: 24185424]
78. Williams C, Chen W, Lee CH, Yaeger D, Vyleta NP, and Smith SM (2012). Coactivation of multiple tightly coupled calcium channels triggers spontaneous release of GABA. Nat. Neurosci 15, 1195–1197. 10.1038/nn.3162. [PubMed: 22842148]
79. Wang CS, Monteggia LM, and Kavalali ET (2023). Spatially non-overlapping Ca2+ signals drive distinct forms of neurotransmission. Cell Rep. 42, 113201. 10.1016/J.CELREP.2023.113201. [PubMed: 37777959]
80. Sabatini BL, and Svoboda K (2000). Analysis of calcium channels in single spines using optical fluctuation analysis. Nature 408, 589–593. 10.1038/35046076. [PubMed: 11117746]
81. Kavalali ET, Zhuo M, Bito H, and Tsien RW (1997). Dendritic Ca2+ channels characterized by recordings from isolated hippocampal dendritic segments. Neuron 18, 651–663. 10.1016/S0896-6273(00)80305-0. [PubMed: 9136773]
82. Markram H, Helm PJ, and Sakmann B (1995). Dendritic calcium transients evoked by single back-propagating action potentials in rat neocortical pyramidal neurons. J. Physiol 485, 1–20. 10.1113/JPHYSIOL.1995.SP020708. [PubMed: 7658365]
83. Westenbroek RE, Sakurai T, Elliott EM, Hell JW, Starr TV, Snutch TP, and Catterall WA (1995). Immunochemical identification and subcellular distribution of the alpha 1A subunits of brain calcium channels. J. Neurosci 15, 6403–6418. 10.1523/JNEUROSCI.15-10-06403.1995. [PubMed: 7472404]
84. Lin Y, McDonough SI, and Lipscombe D (2004). Alternative Splicing in the Voltage-Sensing Region of N-Type CaV2.2 Channels Modulates Channel Kinetics. J. Neurophysiol 92, 2820–2830. 10.1152/jn.00048.2004. [PubMed: 15201306]
85. Iwasaki S, and Takahashi T (1998). Developmental changes in calcium channel types mediating synaptic transmission in rat auditory brainstem. J. Physiol 509, 419–423. 10.1111/j.1469-7793.1998.419bn.x. [PubMed: 9575291]
86. Iwasaki S, Momiyama A, Uchitel OD, and Takahashi T (2000). Developmental changes in calcium channel types mediating central synaptic transmission. J. Neurosci 20, 59–65. 10.1523/JNEUROSCI.20-01-00059.2000. [PubMed: 10627581]
87. Todorov B, van de Ven RCG, Kaja S, Broos LAM, Verbeek SJ, Plomp JJ, Ferrari MD, Frants RR, and van den Maagdenberg AMJM (2006). Conditional inactivation of the Cacna1a gene in transgenic mice. Genesis 44, 589–594. 10.1002/dvg.20255. [PubMed: 17146767]
88. Pereverzev A, Mikhna M, Vajna R, Gissel C, Henry M, Weiergräber M, Hescheler J, Smyth N, and Schneider T (2002). Disturbances in Glucose-Tolerance, Insulin-Release, and Stress-Induced Hyperglycemia upon Disruption of the Cav2.3 (α1E) Subunit of Voltage-Gated Ca2+ Channels. Mol. Endocrinol 16, 884–895. 10.1210/mend.16.4.0801. [PubMed: 11923483]
89. Liu C, Bickford LS, Held RG, Nyitrai H, Südhof TC, and Kaeser PS (2014). The active zone protein family ELKS supports Ca2+ influx at nerve terminals of inhibitory hippocampal neurons. J. Neurosci 34, 12289–12303. 10.1523/JNEUROSCI.0999-14.2014. [PubMed: 25209271]

90. Schindelin J, Arganda-Carreras I, Frise E, Kaynig V, Longair M, Pietzsch T, Preibisch S, Rueden C, Saalfeld S, Schmid B, et al. (2012). Fiji: an open-source platform for biological-image analysis. Nat. Methods 9, 676–682. 10.1038/nmeth.2019. [PubMed: 22743772]

91. Liu C, Kershberg L, Wang J, Schneeberger S, and Kaeser PS (2018). Dopamine Secretion Is Mediated by Sparse Active Zone-like Release Sites. Cell 172, 706–718.e15. 10.1016/j.cell.2018.01.008. [PubMed: 29398114]

92. Xu W, and Lipscombe D (2001). Neuronal Ca(V)1.3alpha(1) L-type channels activate at relatively hyperpolarized membrane potentials and are incompletely inhibited by dihydropyridines. J. Neurosci 21, 5944–5951. 10.1523/JNEUROSCI.21-16-05944.2001. [PubMed: 11487617]

93. Wong MY, Liu C, Wang SSH, Roquas ACF, Fowler SC, and Kaeser PS (2018). Liprin-α3 controls vesicle docking and exocytosis at the active zone of hippocampal synapses. Proc. Natl. Acad. Sci. USA 115, 2234–2239. 10.1073/pnas.1719012115. [PubMed: 29439199]

94. Emperador-Melero J, de Nola G, and Kaeser PS (2021). Intact synapse structure and function after combined knockout of PTPδ, PTPσ and LAR. Elife 10, e66638,2021.01.17.427005. 10.1101/2021.01.17.427005. [PubMed: 33656439]

95. Tan C, de Nola G, Qiao C, Imig C, Born RT, Brose N, and Kaeser PS (2022). Munc13 supports fusogenicity of non-docked vesicles at synapses with disrupted active zones. Elife 11, e79077, 2022.04.01.486686. 10.7554/eLife.79077. [PubMed: 36398873]

Highlights

- $Ca_V2.1$ s, but not $Ca_V1.3$s, are at the active zone and trigger neurotransmitter release
- Swapping the $Ca_V2.1$ C-terminus onto $Ca_V1.3$ confers active zone targeting to $Ca_V1.3$
- $Ca_V1.3$ with the $Ca_V2.1$ C-terminus mediates release that is L-type blocker sensitive
- The first EF hand in the C-terminus is required for $Ca_V2.1$ active zone targeting

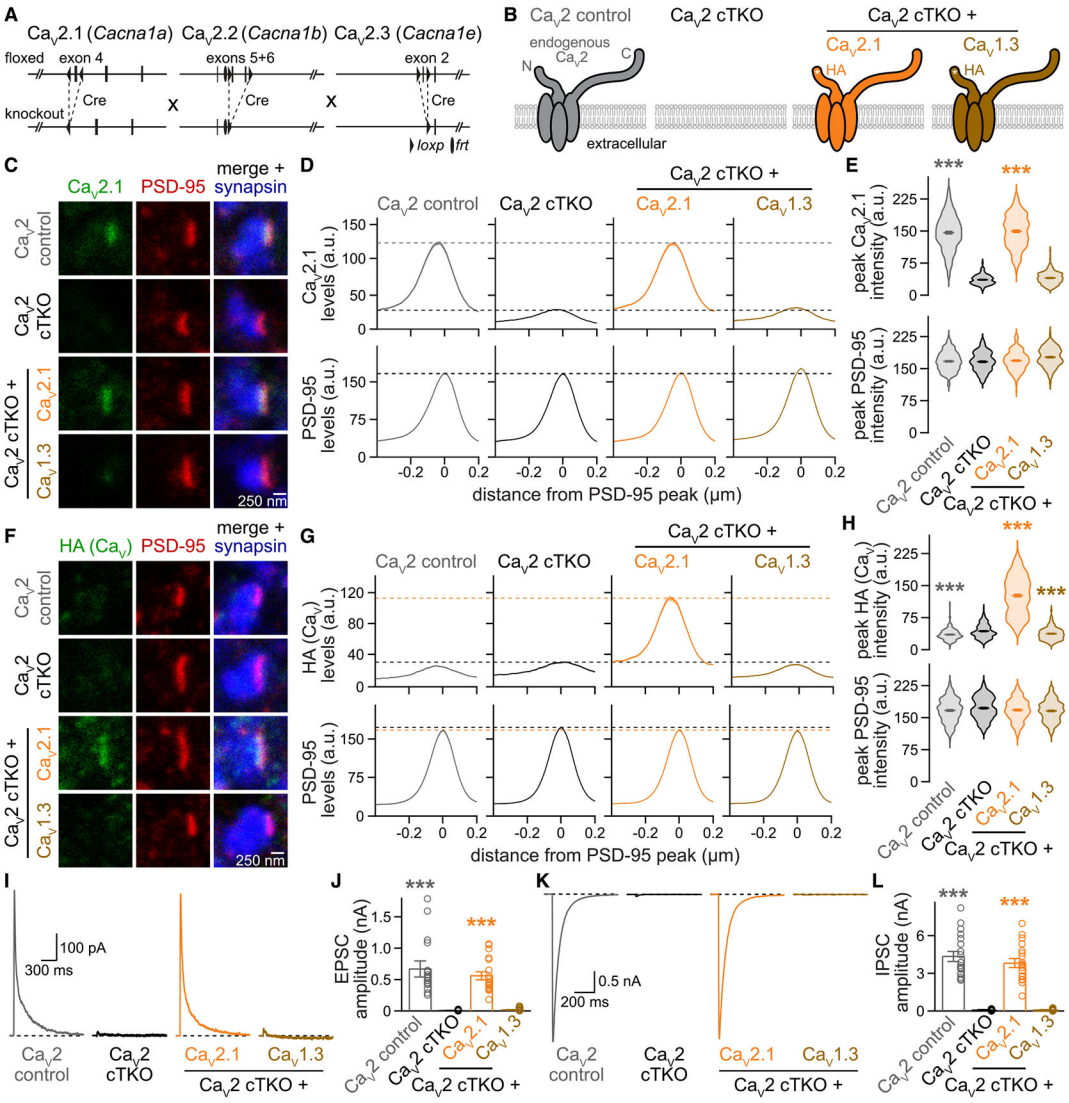

Figure 1. Lentivirally expressed $Ca_V2.1$, but not $Ca_V1.3$, localizes to active zones and restores synaptic transmission in Ca_V2 triple knockout neurons

(A) Strategy for Ca_V2 triple knockout in cultured hippocampal neurons as described before.[20] Transduction of neurons from triple-floxed mice with a lentivirus expressing Cre recombinase produced Ca_V2 cTKO neurons. Ca_V2 control neurons were identical except for the expression of a truncated, recombination-deficient Cre.

(B) Schematic of the conditions for comparison (schematics similar to that in Held et al.[20]); HA-tagged (HA) Ca_Vs were expressed by lentiviral transduction.

(C–E) Representative images (C) and summary plots of intensity profiles (D) and peak levels (E) of $Ca_V2.1$ and PSD-95 at side-view synapses; levels are shown in arbitrary units (a.u.). Neurons were stained with antibodies against $Ca_V2.1$ (analyzed by STED microscopy), PSD-95 (STED), and synapsin (confocal). Dashed lines in (D) denote levels in Ca_V2 cTKO (black) and Ca_V2 control (gray); Ca_V2 control, 195 synapses/3 cultures; Ca_V2 cTKO, 202/3; Ca_V2 cTKO + $Ca_V2.1$, 205/3; Ca_V2 cTKO + $Ca_V1.3$, 201/3.

(F–H) As in (C)–(E) but for synapses stained with antibodies against HA (to detect lentivirally expressed Ca_Vs, STED), PSD-95 (STED), and synapsin (confocal). Dashed lines in (G) denote levels in Ca_V2 cTKO (black) and Ca_V2 cTKO + $Ca_V2.1$ (orange); Ca_V2 control, 208/3; Ca_V2 cTKO, 222/3; Ca_V2 cTKO + $Ca_V2.1$, 227/3; Ca_V2 cTKO + $Ca_V1.3$, 214/3.

(I and J) Representative traces (I) and quantification (J) of NMDAR-mediated EPSCs recorded in whole-cell configuration and evoked by focal electrical stimulation; 18 cells/3 cultures each.

(K and L) As in (I) and (J) but for IPSCs; 18/3 each.

Data are mean ± SEM; ***$p < 0.001$. Statistical significance compared to Ca_V2 cTKO was determined with Kruskal-Wallis tests followed by Dunn's multiple comparisons post hoc tests for the proteins of interest or amplitudes in (E), (H), (J), and (L). In (H), the small decreases in HA intensity in Ca_V2 control and Ca_V2 cTKO + $Ca_V1.3$ compared to Ca_V2 cTKO (which does not express an HA-tagged protein) are unlikely biologically meaningful. For Ca_V C-terminal sequences and additional Ca_V expression analyses, see Figure S1.

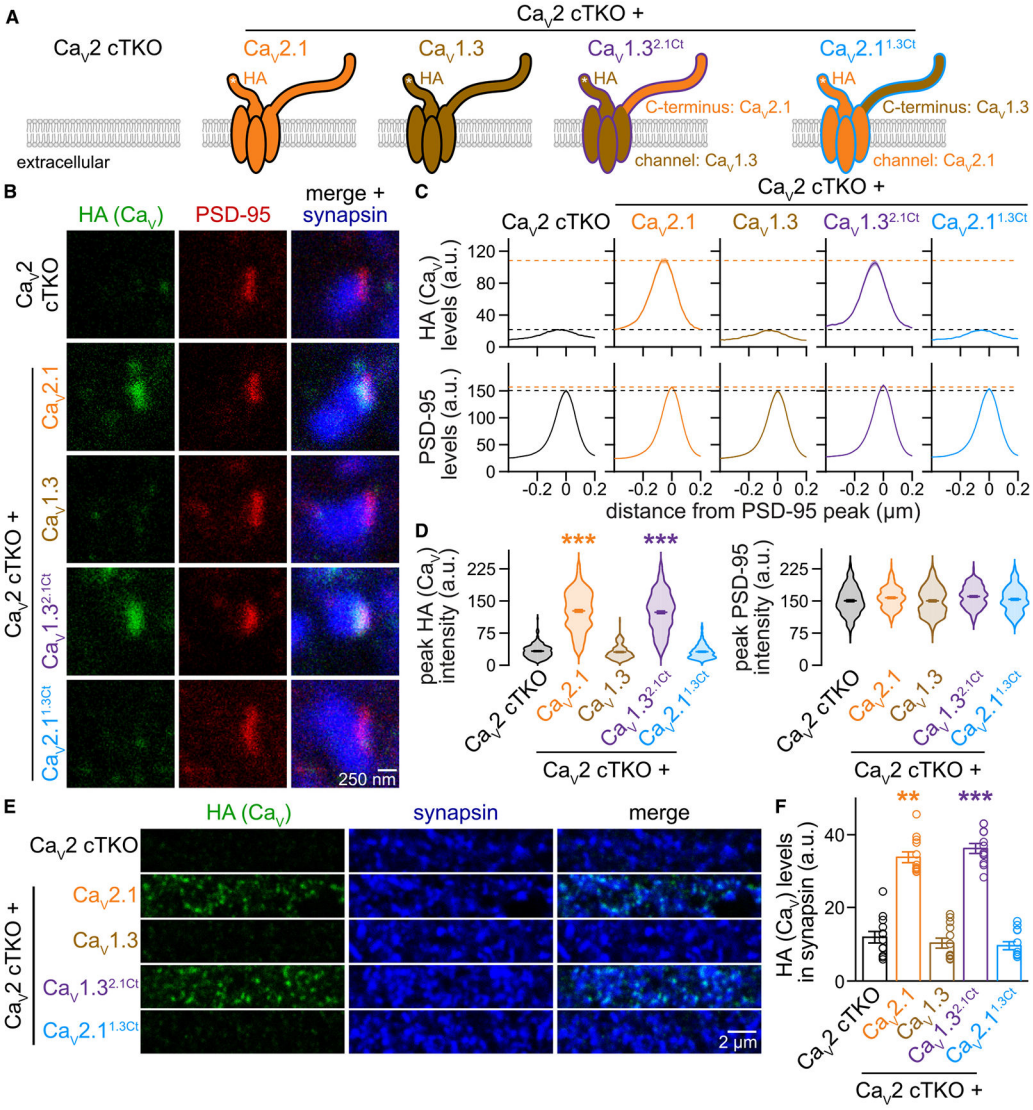

Figure 2. The $Ca_V2.1$ C-terminus suffices to target $Ca_V1.3$ to the presynaptic active zone

(A) Schematic of the conditions for comparison.

(B–D) Representative images (B) and summary plots of intensity profiles (C) and peak levels (D) of HA and PSD-95 at side-view synapses stained for HA (STED), PSD-95 (STED), and synapsin (confocal). Dashed lines in (C) denote levels in Ca_V2 cTKO (black) and Ca_V2 cTKO + $Ca_V2.1$ (orange); Ca_V2 cTKO, 205 synapses/3 cultures; Ca_V2 cTKO + $Ca_V2.1$, 203/3; Ca_V2 cTKO + $Ca_V1.3$, 222/3; Ca_V2 cTKO + $Ca_v1.3^{2.1Ct}$, 218/3; Ca_V2 cTKO + $Ca_V2.1^{1.3Ct}$, 208/3.

(E and F) Representative areas of confocal images (E) and quantification (F) of HA levels in synapsin regions of interest (ROIs). Identical areas (58.14 × 58.14 μm^2) were imaged for confocal (E) and (F) and STED (B)–(D) analyses, and whole images were quantified in (E) and (F); 12 images/3 cultures each.

Data are mean ± SEM; $^{**}p < 0.01$ and $^{***}p < 0.001$. Statistical significance compared to Ca_V2 cTKO was determined with Kruskal-Wallis tests followed by Dunn's multiple

comparisons post hoc tests for the protein of interest in (D) and (F). For additional Ca_V expression analyses, see Figure S2.

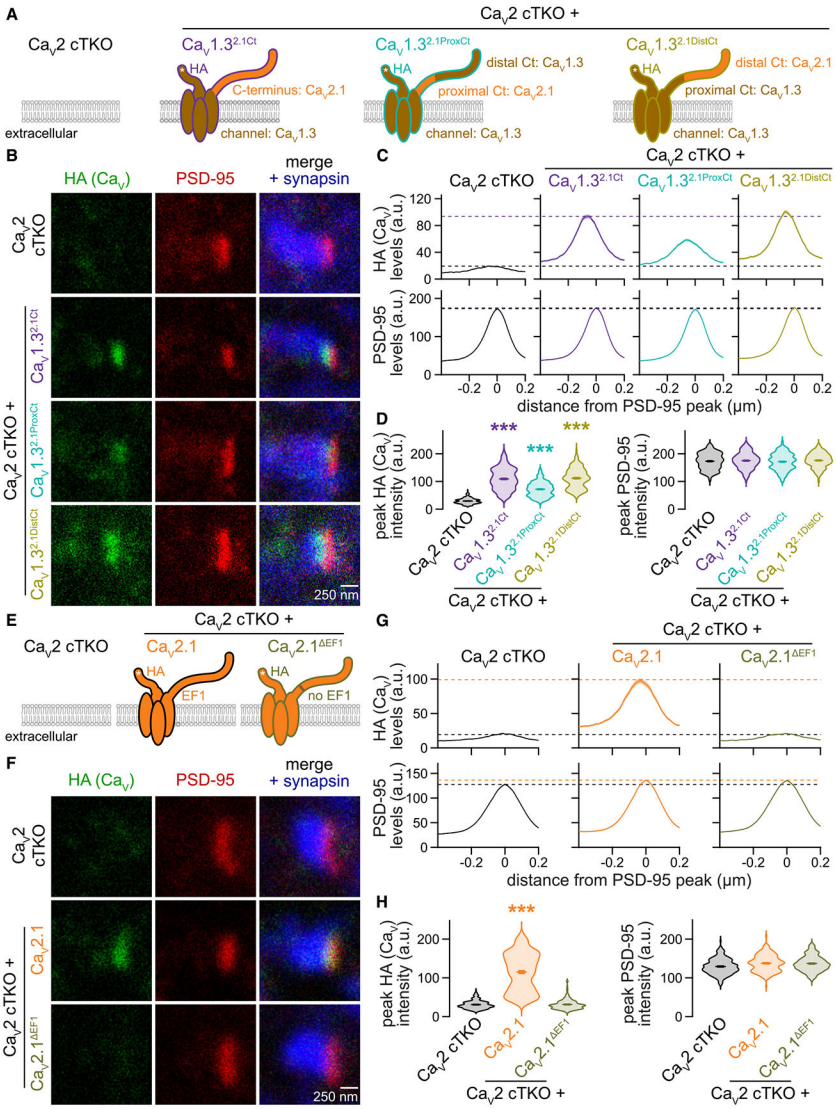

Figure 3. The first EF hand in the proximal C-terminus is essential for Ca$_V$2 active zone targeting

(A) Schematic of the conditions for comparison in (B)–(D).

(B–D) Representative images (B) and summary plots of intensity profiles (C) and peak levels (D) of HA and PSD-95 at side-view synapses stained for HA (STED), PSD-95 (STED), and synapsin (confocal). Dashed lines in (C) denote levels in Ca$_V$2 cTKO (black) and Ca$_V$2 cTKO + Ca$_V$1.3$^{2.1Ct}$ (purple); Ca$_V$2 cTKO, 207 synapses/3 cultures; Ca$_V$2 cTKO + Ca$_V$1.3$^{2.1Ct}$, 204/3; Ca$_V$2 cTKO + Ca$_V$1.3$^{2.1ProxCt}$, 209/3; Ca$_V$2 cTKO + Ca$_V$1.3$^{2.1DistCt}$, 210/3.

(E) Schematic of the conditions for comparison in (F)–(H).

(F–H) Representative images (F) and summary plots of intensity profiles (G) and peak levels (H) of HA and PSD-95 at side-view synapses stained for HA (STED), PSD-95 (STED), and synapsin (confocal). Dashed lines in (G) denote levels in Ca$_V$2 cTKO (black) and Ca$_V$2 cTKO + Ca$_V$2.1 (orange); Ca$_V$2 cTKO, 200/3; Ca$_V$2 cTKO + Ca$_V$2.1, 180/3; Ca$_V$2 cTKO + Ca$_V$2.1^{ΔEF1}, 203/3.

Data are mean ± SEM; ***$p < 0.001$. Statistical significance compared to Ca_V2 cTKO was determined with Kruskal-Wallis tests followed by Dunn's multiple comparisons post hoc tests for the protein of interest in (D) and (H). For additional Ca_V expression analyses, see Figure S3.

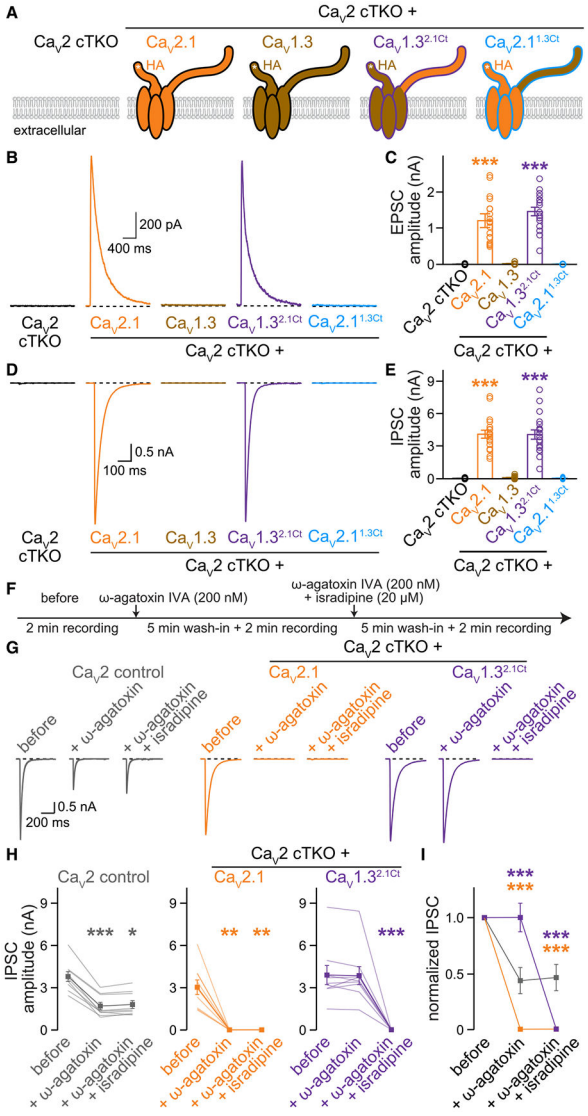

Figure 4. Ca$_V$1.3$^{2.1Ct}$ channels mediate neuro-transmitter release and render it L-type blocker sensitive

(A) Schematic of the conditions for comparison.

(B and C) Representative traces (B) and quantification (C) of NMDAR-mediated EPSCs; 18 cells/3 cultures each.

(D and E) As in (B) and (C) but for IPSCs; 18/3 each. (F) Experimental strategy to evaluate blocker sensitivity of synaptic transmission. Evoked IPSCs were recorded before blocker application (before), after wash-in of 200 nM ω-agatoxin IVA alone (+ ω-agatoxin, to block Ca$_V$2.1), and after wash-in of 200 nM ω-agatoxin IVA and 20 μM isradipine (+ ω-agatoxin + isradipine, to block Ca$_V$1s and Ca$_V$2.1).

(G and H) Representative traces (G) and quantification (H) of IPSCs recorded as outlined in (F); 9/3 each. (I) Comparison of IPSCs normalized to “before” in each condition; 9/3 each. Data are mean ± SEM; *$p < 0.05$, **$p < 0.01$, and ***$p < 0.001$. Statistical significance compared to Ca$_V$2 cTKO was determined with Kruskal-Wallis tests followed by Dunn’s multiple comparisons post hoc tests in (C) and (E). Statistical significance compared to

"before" was determined with Friedman tests followed by Dunn's multiple comparisons post hoc tests in (H). Statistical significance compared to Ca_V2 control was determined with two-way, repeated-measures ANOVA followed by Dunnett's multiple comparisons post hoc tests in (I). For additional electrophysiological data, see Figure S4. For characterization of C-terminally truncated $Ca_V1.3$, see Figure S5.

KEY RESOURCES TABLE

REAGENT of RESOURCE	SOURCE	IDENTIFIER
Antibodies		
rabbit anti-$Ca_V2.1$ (lab antibody code (LAC): A46)	Synaptic Systems	Cat#: 152203 RRID: AB_2619841
mouse IgG1 anti-HA (LAC: A12)	Biolegend	Cat#: 901501 RRID: AB_2565006
guinea pig anti-PSD-95 (LAC: A5)	Synaptic Systems	Cat#: 124014 RRID: AB_2619800
rabbit anti-synapsin (LAC: A30)	Abcam	Cat#: ab8 RRID: AB_2200097
mouse IgG1 anti-synapsin (LAC: A57)	Synaptic Systems	Cat#: 106001 RRID: AB_2617071
mouse IgG2b anti-NeuN (LAC: A254)	Abcam	Cat#: ab104224 RRID: AB_10711040
mouse IgG1 anti-β-actin (LAC: A127)	Sigma	Cat#: A1978 RRID: AB_476692
goat anti-mouse IgG1 Alexa Fluor 488 (LAC: S7)	ThermoFisher	Cat#: A-21121 RRID: AB_2535764
goat anti-guinea pig Alexa Fluor 555 (LAC: S23)	ThermoFisher	Cat#: A-21435 RRID: AB_2535856
goat anti-rabbit Alexa Fluor 633 (LAC: S33)	ThermoFisher	Cat#: A-21070 RRID: AB_2535731
goat anti-rabbit Alexa Fluor 488 (LAC: S5)	ThermoFisher	Cat#: A-11034 RRID: AB_2576217
goat anti-mouse IgG1 Alexa Fluor 633 (LAC: S29)	ThermoFisher	Cat#: A-21126 RRID: AB_2535768
goat anti-mouse IgG1 Alexa Fluor 555 (LAC: S19)	ThermoFisher	Cat#: A-21127 RRID: AB_2535769
goat anti-mouse IgG2b Alexa Fluor 633 (LAC: S31)	ThermoFisher	Cat#: A-21146 RRID: AB_1500899
goat anti-mouse peroxidase-conjugated (LAC: S52)	MP Biomedicals	Cat#: 0855550 RRID: AB_2334540
goat anti-rabbit peroxidase-conjugated (LAC: S53)	MP Biomedicals	Cat#: 0855676 RRID: AB_2334589
Chemicals, Peptides and Recombinant Proteins		
Picrotoxin (PTX)	Tocris	Cat#: 1128
D-2-amino-5-phosphonopentanoic acid (D-AP5)	Tocris	Cat#: 0106
6-Cyano-7-Nitroquinoxaline-2,3-dione (CNQX)	Tocris	Cat#: 0190
QX314-Cl	Tocris	Cat#: 2313
ω-Agatoxin IVA	Alomone	Cat#: STA-500
Isradipine	Tocris	Cat#: 2004
Tetrodotoxin (TTX)	Tocris	Cat#: 1078
Experimental Models: Cell Lines		
HEK293T	ATCC	Cat#: CRL-3216 RRID:CVCL_0063
Experimental Models: Organisms/Strains		
$Ca_V2.1$ (*Cacna1a*) conditional knockout	Todorov et al.[87]	N/A

REAGENT of RESOURCE	SOURCE	IDENTIFIER
$Ca_V2.2$ (*Cacna1b*) conditional knockout	Held et al.[20]	Cat# KOMP: CSD34514 RRID: MMRRC_046864-UCD
$Ca_V2.3$ (*Cacna1e*) conditional knockout	Pereverzev et al.[88]	N/A
Recombinant DNA		
pFSW EGFP-ΔCre (lab plasmid code (LPC): p010)	Liu et al.[89]	N/A
pFSW EGFP-Cre (LPC: p009)	Liu et al.[89]	N/A
pREV (LPC: 023)	Liu et al.[89]	N/A
pRRE (LPC: 024)	Liu et al.[89]	N/A
pVSVG (LPC: 025)	Liu et al.[89]	N/A
pFSW (LPC: 008)	Liu et al.[89]	N/A
pCMV HA-$Ca_V2.1$ (LPC: p771)	Held et al.[20]	N/A
pCMV HA-$Ca_V2.1^{\Delta EF1}$ (LPC: p939)	this study	N/A
pCMV HA-$Ca_V1.3$ (LPC: p1073)	this study	N/A
pCMV HA-$Ca_V1.3^{2.1Ct}$ (LPC: p1074)	this study	N/A
pCMV HA-$Ca_V2.1^{1.3Ct}$ (LPC: p1075)	this study	N/A
pCMV HA-$Ca_V1.3^{\Delta Ct}$ (LPC: p1076)	this study	N/A
pCMV HA-$Ca_V1.3^{2.1ProxCt}$ (LPC: p1081)	this study	N/A
pCMV HA-$Ca_V1.3^{2.1DistCt}$ (LPC: p1082)	this study	N/A
pMT2 $Ca_V\beta1b$-GFP (LPC: p754)	Page et al.[36]	Cat#: 89893 RRID: Addgene_89893
pCNDA3.1 $Ca_V\alpha2\delta$-1 (LPC: p752)	Lin et al.[84]	Cat#: 26575 RRID: Addgene_26575
pFSW HA-$Ca_V2.1$ (LPC: p789)	Held et al.[20]	N/A
pFSW HA-$Ca_V2.1^{\Delta EF1}$ (LPC: p947)	this study	N/A
pFSW HA-$Ca_V1.3$ (LPC: p1077)	this study	N/A
pFSW HA-$Ca_V1.3^{2.1Ct}$ (LPC: p1078)	this study	N/A
pFSW HA-$Ca_V2.1^{1.3Ct}$ (LPC: p1079)	this study	N/A
pFSW HA-$Ca_V1.3^{\Delta Ct}$ (LPC: p1080)	this study	N/A
pFSW HA-$Ca_V1.3^{2.1ProxCt}$ (LPC: p1083)	this study	N/A
pFSW HA-$Ca_V1.3^{2.1DistCt}$ (LPC: p1084)	this study	N/A
Oligonucleotides		
Cacna1a forward primer: ACCTACAGTCTGCCAGGAG	Held et al.[20]	N/A
Cacna1a reverse primer: TGAAGCCCAGACATCCTTGG	Held et al.[20]	N/A
Cacna1b forward primer: TGGTTGGTGTCCTGTTCTCC	Held et al.[20]	N/A
Cacna1b reverse primer: TAAGGAGCAGGGAATCCTGG	Held et al.[20]	N/A
Cacna1e forward primer: GACAAGACCCCAATGTCTCG	Held et al.[20]	N/A
Cacna1e reverse primer: TCCATGTTCCTTCTCACTCC	Held et al.[20]	N/A
Software and Algorithms		
Fiji	Schindelin et al.[90]	RRID: SCR_00228 https://imagej.net/Fiji/Downloads

REAGENT of RESOURCE	SOURCE	IDENTIFIER
Prism9	GraphPad	RRID: SCR_002798 https://www.graphpad.com/scientific-software/prism
pClamp	Molecular Devices	RRID: SCR_011323 https://www.moleculardevices.com/products/software/pclamp.html
MATLAB	MathWorks	RRID: SCR_001622 https://www.mathworks.com/products/matlab.html
MATLAB code for automatic object detection	Tan et al.[95]	https://doi.org/10.5281/zenodo.6388196